INVESTIGATION OF THE EFFECT OF MICRO ARC OXIDATION AND SHOT PEENING ON CORROSION AND WEAR BEHAVIOR OF AZ31-X-LA AND AZ31-X-ND ALLOYS

GALAL ELMENSOURI

2020
PhD THESIS
METALLURGICAL AND MATERIALS ENGINEERING

Thesis Advisor
Prof. Dr. Hayrettin AHLATCI

INVESTIGATION OF THE EFFECT OF MICRO ARC OXIDATION AND SHOT PEENING ON CORROSION AND WEAR BEHAVIOR OF AZ31-xLa and AZ31-xNd ALLOYS

GALAL ELMENSOURI

T.C
Karabuk University
Institute of Graduate Programs
Department of Metallurgical and Materials Engineering
Prepared as PhD Thesis

Thesis Advisor
Prof. Dr. Hayrettin AHLATCI

KARABUK
July 2020

I certify that in my opinion the thesis submitted by Galal ELMENSOURI titled "INVESTIGATION OF THE EFFECT OF MICRO ARC OXIDATION AND SHOT PEENING ON CORROSION AND WEAR BEHAVIOR OF AZ31-xLa and AZ31-xNd ALLOYS" is fully adequate in scope and in quality as a thesis for the degree of PhD.

Prof. Dr. Hayrettin AHLATCI .....
Thesis Advisor, Department of Metallurgical and Materials Engineering

This thesis is accepted by the examining committee with a unanimous vote in the Department of Metallurgical and Materials Engineering as a PhD thesis. 09.07.2020

Examining Committee Members (Institutions)	Signature
Chairman : Prof.Dr. Mustafa ACARER (SU)	.....
Member : Prof.Dr. Hayrettin AHLATCI (KBU)	.....
Member : Assoc.Prof.Dr. Yunus TÜREN (KBU)	.....
Member : Assoc.Prof.Dr. Okan ÜNAL (KBU)	.....
Member : Assoc.Prof.Dr. Ebru Emine ŞÜKÜROĞLU (GU)	.....

The degree of PhD by the thesis submitted is approved by the Administrative Board of the Institute of Graduate Programs, Karabuk University.

Prof. Dr. Hasan SOLMAZ .....
Director of the Institute of Graduate Programs

"I declare that all the information within this thesis has been gathered and presented in accordance with academic regulations and ethical principles and I have according to the requirements of these regulations and principles cited all those which do not originate in this work as well."

Galal Elmensouri

ABSTRACT

M. Sc. Thesis

INVESTIGATION OF THE EFFECT OF MICRO ARC OXIDATION AND SHOT PEENING ON CORROSION AND WEAR BEHAVIOR OF AZ31-xLa AND AZ31-xNd ALLOYS

Galal Elmensouri

Karabük University
Institute of Graduate Programs
The Department of Metallurgical and Materials Engineering

Thesis Advisor:
Prof. Dr. Hayrettin AHLATCI
July 2020, 68 pages

To reduce the CO_2 emission and to increase the energy efficiency, the using of magnesium alloys as a light material in automotive and space industries is important due to their low density of 1,74 g/cm^3 and high specific strength. Moreover, as biomaterial the Mg alloys is an important candidate due to their corrosion resistance could be control thanks to alloying elements or surface modifications. Furthermore, the rare earth metals are the excellent texture modifier and they impart stable microstructure to Mg alloys in which secondary phases resisting extreme corrosion or wear conditions. Besides, shot peening is acceptable method to develop the surface strength of light materials such as aluminum or magnesium. In addition, micro arc oxidation (MAO) can be used as effective way to increase the corrosion and wear resistance of light materials. However, many studies about improving of corrosion or wear resistance of Mg alloys is limited at as-cast materials. In this study, we produced

AZ31 Mg alloys containing Neodymium (Nd) and Lanthanum (La) elements as using of low pressure die casting method, following hot rolling was utilized to obtain 2 mm sheets which deformed at different rolling speed. After the hot rolling, some of the produced sheets was exposed directly MAO or some of them was exposed both shot peening and MAO. To examine the wear and corrosion resistance of materials the wear and corrosion tests were applied at dry condition and 3,5%NaCl solution at 25°C, respectively. The microstructure after coating was characterized by scanning electron microscopy (SEM) and X-ray diffraction (XRD). Further, the surface properties were obtained by profilometer as surface roughness.

Key Words : AZ31(+La, Nd), Hot rolling, Shot peening, MAO, Corrosion, Wear.
Science Code : 91519

ÖZET

Doktora Tezi

MİKRO ARK OKSİDASYON VE BİLYELİ DÖVME İŞLEMLERİNİN AZ31-xLa VE AZ31-xNd MAGNEZYUM ALAŞIMLARININ KOROZYON VE AŞINMA DAVRANIŞLARINA ETKİSİNİN İNCELENMESİ

Galal ELMENSOURI

Karabük Üniversitesi
Lisansüstü Eğitim Enstitüsü
Metalurji ve Malzeme Mühendisliği Anabilim Dalı

Tez Danışmanı:
Prof. Dr. Hayrettin AHLATCI

Temmuz 2020, 68 sayfa

CO_2 emisyonunu azaltmak ve enerji verimliliğini artırmak için, magnezyum alaşımlarının otomotiv ve uzay endüstrilerinde hafif bir malzeme olarak kullanılması, 1,74 g / cm^3 düşük yoğunluğu ve yüksek özgül mukavemeti nedeniyle önemlidir. Ayrıca, biyo-malzeme olarak Mg alaşımları korozyon direncinden dolayı önemli bir adaydır, bu özellik alaşım elementleri veya yüzey modifikasyonları sayesinde kontrol edilebilir. Ayrıca, nadir toprak metalleri mükemmel doku modifiye edicidir ve ikincil fazların aşırı korozyon veya aşınma koşullarına dirençli olduğu Mg alaşımlarına kararlı mikroyapı verir. Buna ilaveten, bilyeli dövme işlemi alüminyum veya magnezyum gibi hafif malzemelerin yüzey mukavemetini geliştirmek için kabul edilebilir bir yöntemdir. Ek olarak, mikro ark oksidasyonu (MAO), hafif malzemelerin korozyonunu ve aşınma direncini arttırmak için etkili bir yol olarak kullanılabilir. Bununla birlikte, Mg alaşımlarının korozyonu veya aşınma direncinin iyileştirilmesi

ile ilgili birçok çalışma döküm malzemelerde sınırlıdır. Bu çalışmada, farklı haddeleme hızlarında deforme olan 2 mm levhalar elde etmek için düşük basınçlı döküm yöntemi kullanılarak Neodyum (Nd) ve Lantan (La) elementleri içeren AZ31 Mg alaşımları ürettik. Sıcak haddeleme işleminden sonra, üretilen saç malzememelerin bir kısmı doğrudan MAO'ya maruz bırakıldı ya da bir kısmı da hem bilyeli dövme hem de MAO'ya maruz bırakıldı. Malzemelerin aşınma ve korozyon direncini incelemek için aşınma ve korozyon testleri sırasıyla 25 ° C'de kuru durumda ve %3,5 NaCl çözeltisi ile uygulanmıştır. Kaplama sonrası mikroyapı, taramalı elektron mikroskopisi (SEM) ve X-ışını kırınımı (XRD) ile karakterize edildi. Ayrıca yüzey özellikleri profilometre ile yüzey pürüzlülüğü olarak elde edilmiştir.

Anahtar Kelimeler : AZ31 (+ La, Nd), Sıcak haddeleme, Bilyeli yüzey dövme, MAO, Korozyon, Aşınma.

Bilim Kodu : 91519

ACKNOWLEDGMENT

I would like to reveal my major thanks of gratitude to my advisor Prof. Dr. Hayrettin AHLATCI who gave me the glorious moment for the extended support of my Ph.D. research and detailed analysis, for his perseverance, interest, and tremendous insight. His direction encouraged great exploration moreover I moved to learn about so many new things. I am absolutely grateful to him. Besides my advisor, I would like to thank the rest of my thesis committee: Dr. Yunus Turan, Dr. Okan Ünal, and Dr. Ebru Emine Sükürоglu and Dr. Ismael Hakki KARA, for their encouragement, insightful comments, and hard questions.

Second, I would like to extend my sincere thanks to the Libyan state, which supported me financially, and also my thanks to the Turkish state and to the Turkish people with whom I lived during the period of my PhD study.

Finally, I would also like to thank my family and my friends who helped me a lot in finalizing this thesis within the limited time frame.

CONTENTS

Page

Page

LIST OF FIGURES

Page

Page

Page

LIST OF TABLES

Page

SYMBOLS AND ABBREVITIONS INDEX

SYMBOLS

gr : gram

cm : centimeter

ABBREVITIONS

MPa : megapascal

log : logarithmic

Mg : Magnesium

GPa : Gigapascal

PART 1

INTRODUCTION

Firstly, as a structure materials steel and aluminum could be replaced by Mg alloys because of their 1,74 g/cm^3 density and high strength per density. As a result of their low density and high strength/density ratio, Mg alloys have engaged noticeable consideration as structural materials for utilizations in automotive and aerospace productions. While as a hexagonal close-packed (hcp) metal, Mg alloys have weak form ability at room condition due to number of self-reliant slipping arrangements. Concerning the Mg alloys, the non-basal slips are comparatively usable, and the plastic deformation is inhibited at room temperature because critical resolved shear stress of a basal plane is far lower than those of the non-basal planes on prismatic and pyramidal planes at low temperatures. Rolling is a good technique of forming Mg alloy; however, some objections emerge as rolling passes are added, smaller single pass reduction, low production and discernible mechanical anisotropy. These objections tremendously hinder the advancement of magnesium alloys. Furthermore, rolling outcomes in a strong basal texture with the c-axis coordinated virtually complementary to the sheet normal direction, which reduces basal slip in consecutive sheet forming. This brings about the high normal anisotropy in sheet, moderate work hardening and, therefore, low values of uniform elongation. Secondly, conventional metal base metallic materials like Ti, Co and Fe alloys have performed an important role in the repair or restoration of rotten or harmed bones as support implants. However, the elastic modulus of these alloys is considerably greater than that of the bone, which causes the implants placed within the bone to reduce bone density in that area, reducing bone tensile strength and drawing in. When compared to conventional metal alloys, a biodegradable material should contain properties that will not cause durable real discomfort but avoid secondary surgery in the removal of implants. Magnesium base metallic combinations as current possible biomaterials have inviting excellent

mechanical properties such as special density (1.7-2.0 g / cm3) and elastic modulus (41-45 GPa) values closest to human bone (1.8-2.1 g / cm3, 10-40 GPa) and thus minimizes the tensile strength in the bone. In addition, magnesium and its alloys are non-toxic and have good biocompatibility. Contrastingly, Mg ions are present in a large quantity in the human body and are link in countless metabolic feedbacks and structures. This means that Mg can be introduced into the human body as a metallic biomaterial, where it is slowly dissolved, consumed or absorbed. Thanks to Mg, adhesion of bone cell develops, and Mg regression has no effect on growth of cell. In contrast, high Mg ion concentration leads to activation of bone cell. However, the degradability of Mg is like a double-edged knife. Mg is a very reactive metal and has a high corrosion rate in physiological solutions. These high corrosion rate values should be under control or reduced if Mg is to be used as biomaterial. To achieve this, the coating can be used as a means of corrosion rate blocking. The rate of corrosion can be reduced to ensure that the metallic integrity remains mechanically as intact during the treatment of the bone. The coating application will also downplay the formation of hydrogen. Hydrogen formation is seen as a potential disadvantage. Normally, the coating will slowly wear out, leading to controlled material degradation.

PART 2

LITERATURE REVIEW

Magnesium (Mg) alloys have been broadly utilized in automotive and aerospace industries due to their low density and high strength/density [1]. Sadly, the application of magnesium alloys is often inhibited by unacceptable corrosion and fatigue properties. Micro arc oxidation (MAO) is most prevailing technique to insulate Mg alloys from corrosion [2]. Lately, innumerable performances have been managed to scrutinize the tracts of nanostructured exterior blankets on Mg alloys [3] and [4]. Research argued the useful influence of nano crystallization on the hardness and fatigue properties [5]. However, in terms of corrosion behavior of nanostructured surface layers on Mg alloys, incompatible outlooks are announced. The medical field is the potential application of Mg alloys due to the Mg alloys can be utilized as an implant for biomaterial. Firstly, the biocompatibility of Mg was introduced in the beginning of 20^{th} century. Nonetheless, the actual accelerated corrosion and hydrogen progress phenomena belonging to Mg forced researchers to discontinue their first clinical operations. Afresh, a better understanding of corrosion mechanisms and the development of creative corrosion protection techniques have restored research concern with biodegradable Mg alloys [6] [7] [8] [9].

2.1. DEFORMATION SYSTEMS IN MAGNESIUM

Hexagonal tight package (HCP) structured Mg alloys have a c / a ratio of 1.624 It was calculated. The most important crystallographic role in the deformation of magnesium planes $\{0001\}$ basal plane, $\{10\bar{1}0\}$ prismatic plane, $\{1011\}$ pyramidal plane and $\{1212\}$ is the second order pyramidal plane. All these planes are given in Figure 2.1 [10] .

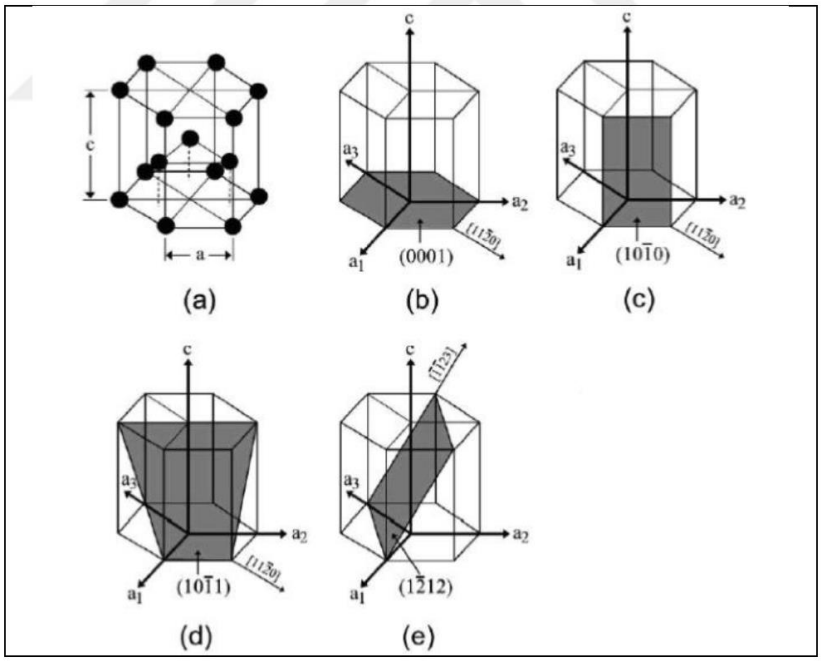

Figure 2.1. a) Mg unit cell, b) basal plane, c) prismatic plane, d) pyramidal and e) the second order pyramidal plane [10].

2.1.1. Slip

Slips in specific crystallographic planes and along certain crystallographic directions dislocations, resulting in atomic displacement. Different slip shifting of associated dislocations in systems (i.e. shear plane and direction), absorbed strains resulting in a constant deformation. According to Taylor in a randomly oriented polycrystalline metal the disclosure. more than five independent sliding systems are needed to achieve deformation. One When the dislocation reaches a grain boundary, the shear system will cannot shift from one to another due to the change in orientation. Therefore, shear to maintain shear activity, to prevent material breakage systems should be available [11] [8]. Volume-centered cubic (BCC) and surface Unlike centric cubic (FCC) crystal structures, HCP crystals meet the Taylor criteria. cannot contribute sufficient separate sliding system to fulfill Critical Strain (CRSS) values of these systems cause this situation [12]. Figure 3.1 shows the planes and directions of the major sliding systems in magnesium shows schematically. Of the four dominant shear systems, three (basal, prismatic and first order pyramid), close to each other direction of sliding <1120> share. Here, three sets of main planes (i) containing shear directions are basal, (ii) and (iii) pyramidal. Activation of these shift systems is only four can provide independent

slip system; any random stretch path it is still insufficient for five of them to accommodate [10]. Mg alloys the most important factor in shaping is temperature. A small number of sliding systems 225 Above ° C prismatic and pyramidal systems are active [13]. Herrera Solaz and arc. 0.5% Nd and 1% Nd (wt. examined the effect. CRSS basal / CRSS twinning ratio constant in 0.5Nd alloy remains but increased in 1Nd alloy, CRSS pyrasma / CRSS twinning and CRSS Pyramid / CRSS twinning ratio decreased after 0.5% Nd and 1% Nd alloy have been [14].

2.1.2. Twins

Twinning is the second time a metallic material exhibits during deformation as a mechanism. Particularly difficult to slip materials show twinning. There is no change in the crystal structure as a result of twinning but there is a change in the crystal lattice direction. Unlike atoms seen in shear they are displaced at the interatomic distance relative to each other. Single crystal twinning shared structure and original crystal. It remains. Twinning lattices are like the reflection of the original lattice in the mirror and The plane of symmetry between them is defined as the twin plane [8]. Twinning studies in the literature, it is divided into tensile and compression twinning. Elongation of crystalline c- along the axis {10-12} or by pull twinning. Tensile stresses along the c-axis or compression stress perpendicular to the c-axis occurs when applied [15]. Compression twins are {11-22} and {10-11}is created by [16]. Meng Y. et al. rupture usually it has been reported to occur by twins or slip bands [17]. Twin here formation and the highest local strain causes rupture [18].

2.1.3. Dynamic Recrystallization (DRX)

In metals where the softening rate is slow (ie, with low or medium stacking error energy), DRX may occur when a detracting deformation situation is signed in. As shown in Figure 3.5, the flow curve of a DRX treated material generally shows a broad peak [19]. The distinctive regions of the curve in Figure 3.4 are: 1. Dislocation intensity increases with stress during the first stages of deformation; When the stored energy reaches a critical value, the DRX starts with a critical strain (ε_c) before the peak (ε_p) of the flow curve. 2. Post-peak flow smoothing due to the progression of DRX and

the formation of new particles deformed during deformation. Dynamic recrystallization occurs during the thermomechanical processes of Mg alloys, which contributes to wear and the formation of a finer microstructure. Numerous studies have been attended on the mechanisms of DRX in Mg alloys, which can be categorized into three different types: continuous (sub) DRX and discontinuous (bulging) DRX [19].

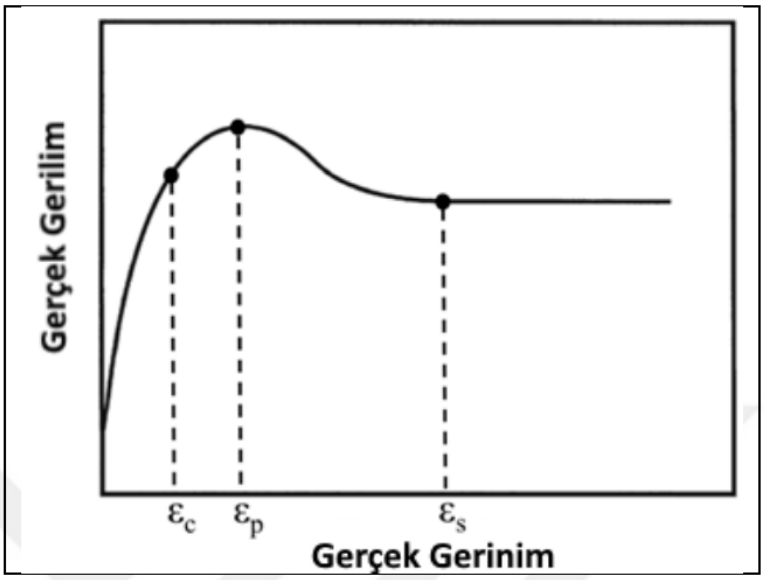

Figure 2.2. Typical stress-strain curve with dynamic recrystallization [42].

It is desirable to weaken the basal texture (0002) during rolling. However, DRX (0002) has been reported to have little effect on attenuation of the basal test [20]. The effect of rolling speed on DRX formation is quite high. It was reported that AZ31 Mg alloy, which was rolled at 400 ° C at 470 m / min rolling speed, first formed the twinning and then DRXs formed due to the twinning and also the fine-grained twins gained more place with increasing deformation rate. DRXs, especially formed on twin bands, have been reported to have smaller grains, lower internal stresses and weaker textures [21].

2.2. CORROSION RATE BEHAVIOUR OF MG ALLOYS

The thermodynamics of pure Mg is a base for appreciation the electrochemical corrosion of Mg compositions. The Mg balance in miscellaneous surroundings can also support advise for reckoning the corrosion rating of Mg alloys in typical statutes

which is accessible against understanding the thermodynamic behavior of Mg alloys. This meaning Mg in usual surroundings has an excellent trend to instinctively convert into its oxidized describes. Proportionately, if Mg is opened to environments including oxygen or water, its external section always leans to be very quickly oxidized, so that occurring an oxide or hydroxide surface film. Virtually there are many determinants that can influence the corrosive reactions and thus also induce the corrosion of Mg. For instance, the existence of oxygen in water can lead to greater or less oxygen decline on Mg which may have some effect on the cathodic and anodic polarization behaviors of Mg, especially in atmospheric surroundings where the amount of oxygen is sufficient.

2.2.1. The Surface Film and Coating of Mg Alloys

The surface of metal could be oxide in natural surroundings which gives rise to covering of oxide film or hydroxide film. Mg and its alloys be apt to be dissolved and oxidized in most possible surroundings. Subsequent corrosion products can deposit and form a surface film on its surface.

Plasma electrolytic oxidation (PEO) is an alluring engineering of surface processing for Mg compositions. Amid PEO, the Mg surface is swapping a ceramic coating stiffly using huge discharges of electric energy. This can attempt developed wear and corrosion resistance to different magnesium components, thus enlarging their areas of application. MAO is an extreme-voltage plasma-supported anodic oxidation method, commonly used for surface modifications of Mg and alloys. The plasma charge discharge in the course of the MAO process leads to limited momentary liquefying of the oxide layer and forms a highly sticky ceramic oxide coating. The MAO coating gives high hardness, good wear resistance and average corrosion resistance and better warm condition stability and non-conductivity of electric properties. The evolution of the MAO coating on Mg and its alloys first begins amidst the dissolution of the metal and the growing of the film of barrier. At this stage, the voltage shows a rapid and linear increase. The main force is provided by the electric field in transporting the positive ions and negative ions contained in the electrolyte through the barrier film and increases the thickness of the film at 0.6nm / V. The barrier film forming is escorted

by the development of O_2. This step shows the ordinary anodic coating process. In the initial moments of barrier film expansion, a homogeneous flow of current occurs along the film. However, when 100-200 nm thickness was observed on the film, it starts to show a resistance to current. Subsequently, in some regions of the barrier film, the insulating property is reduced and there is less resistance there, and thus the formation of discharge in the form of fine sparks begins. The voltage value at which this event occurs gives the breaking voltage. After this stage, the cell voltage starts to upsurge frequently. At this leg, the flow of prevailing only condenses in the fracture zones and leads to regional thickness increase. The formation of the fresh layer of coating revitalizes the resistance to current flow while the other parts tend to break because they are less resistant. Thus, too many fine white sparks are randomly dispersed and move rapidly over the entire anode surface. Mg implant materials treated with MAO give positive results in bone repair. Y Wu et al. MAO applied with different coating thickness compared to pure Mg alloy Mg alloys showed better biocompatibility. It is an advantage that the MAO coated Mg alloy provides slower gas formation during bone repair, and the rate of gas formation decreases with increasing coating thickness. In addition, MAO applied Mg implant material showed faster development in the first stage of cell adhesion and spread. In addition, the degradation time of the implant material is increased during treatment with MAO, where the rate of $Mg(OH)_2$ occurring is reduced, increasing the degradation time of the implant material. Surface roughness has an impact on the nucleation and development of the barrier film during the MAO process. Nashrah et al. The roughness of surface values of sheet AZ31 Mg alloy were obtained by using fine and coarse sanding to be 0.025μm and 1μm respectively, and then two materials were subjected to MAO treatment. The fracture voltage of the material having a high surface roughness was earlier than that where nucleation was more easily started in ridge areas. The performed electrochemical corrosion measurements showed that the MAO coating of the starting material with high surface roughness showed twice the polarization resistance due to the perforated structure. The large-perforated structure provides room for chemically interlocking secondary materials, thus contributing to corrosion resistance [22].

2.3. WEAR BEHAVIOUR OF MG ALLOYS

Description of wear is described as the loss of material caused by sliding, impact or rolling between two solid surfaces. Adhesive wear (see figure 2.3); type of wear that causes material transfer between two solids as a result of adhesive forces [23].

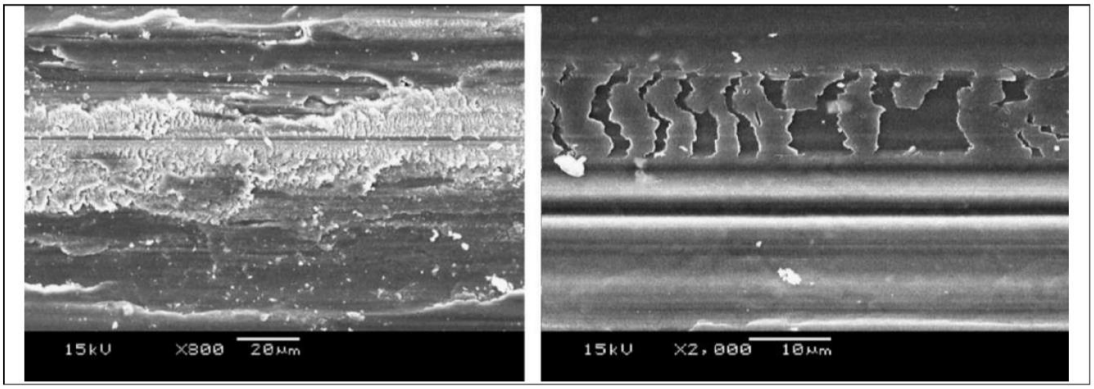

Figure 2.3. Figure Adhesive Wear SEM images [23].

Abrasive wear (see figure 2.4); it is caused by rubbing a solid material against a material that is harder or of the same hardness [24]. It shows itself in the constitute of grooves and scratches in the way of wear. Here, the more rigid counter-material causes abrasion of striped particles from the surface [25].

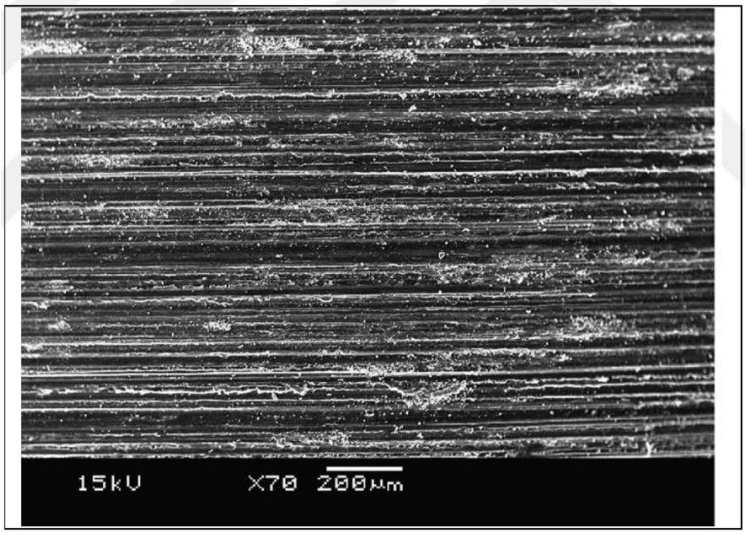

Figure 2.4. SEM Image of abrasive wear [23].

Oxidation: The presence of molten particles caused by heating during wear leads to oxidation wear (see figure 2.5). During continued wear, the oxide particles are dispersed in the worn cavities and adhere to each other. Here, the contact between the primary material and the abrasive material is reduced and consequently the wear rate is reduced [25].

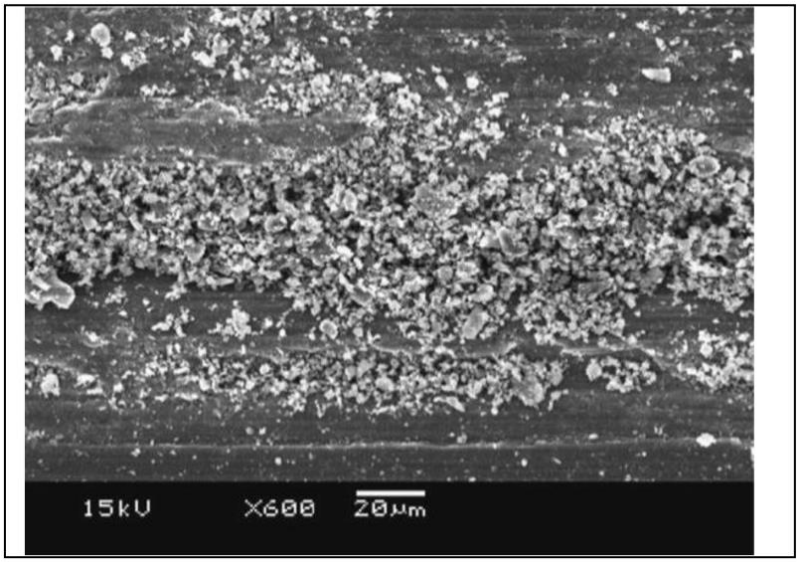

Figure 2.5. SEM Image of oxidation wear [23].

Thermal softening and Melting; high wear rate during the wear or heat caused by heavy load causes the material to wear in bulk. In addition, there is a significant increase in wear rate in this environment. This case occurs especially in Mg alloys [26].

Delamination wear: in the form of short cracks in the approach perpendicular to the wear direction (see figure 2.6). Leaf-like particles cause creases to form over time [26] [22].

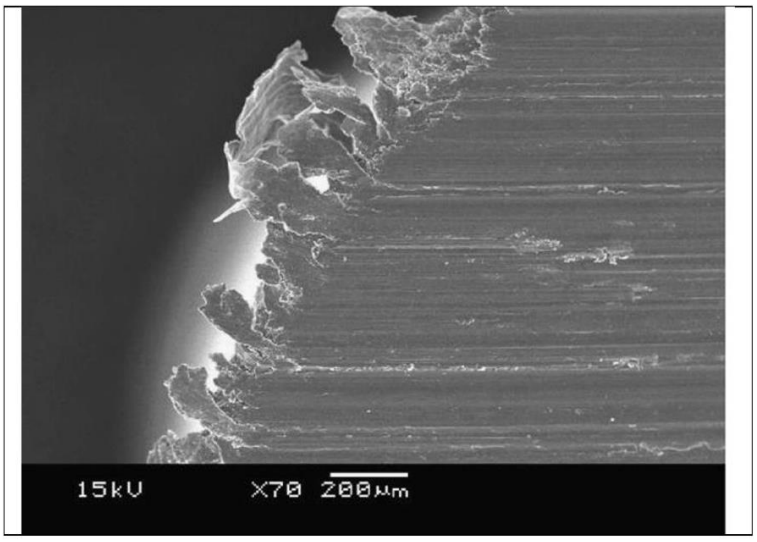

Figure 2.6. SEM image of delamination wear [23].

2.3.1. Effect of Rare Earth Metals, MAO and Shot Peening on Wear Behavior of Mg Alloys

Micro arc oxidation process depends on selected parameters to 1000 V (and approximately 1 MW in capacity) needs. This high energy is dangerous depending on the type and size of parts creates a production process. Given the amount of energy used micro arc production costs in the oxidation process to traditional anodic oxidation methods more than that. In addition, high temperature formed on the exterior section of the material high capacity for cooling the solution used in the process. Refrigerant will be needed. The ceramic coating formed as a result of the process is rough and it is very brittle, so its abrasion resistance is very low on the outermost surface. The inner layers of the ceramic coating have the opposite property. These layers it is quite hard and has high abrasion resistance. But on the surface of the material removal of the top layer of this ceramic coating is both cost effective and is not efficient in terms of production. Many advantages of micro arc oxidation Besides the above-mentioned disadvantages, the use of this technology limits.

Liang and et.al. studied AM60 B grade magnesium alloy, silica-based and phosphate based on two separate electrolytes and the effect of electrolyte on the MAO process aimed to research. Silica based Na2SiO3 + KOH mixture, Phosphate based on Na3PO4 + KOH mixture. Two equal times When comparing the results of the

experiment, phosphate-based electrolyte degradation and critical higher than the end voltage at the same time. They have determined that. When compared morphological properties, silica-based Electroplated coating is more homogeneous and compact, phosphate-based they found that the coating obtained by electrolyte was more porous. Alkali silicate MgO and Mg2SiO4 phases in the material structure. in the process using phosphate solution, only MgO phase is formed. It has been identified. Nonetheless, when formed layer hardness is examined, a layer of silicate solution with a higher hardness than a phosphate solution formation. This is because the Mg2SiO4 phase compared to the MgO phase more rigid. Coating obtained with alkaline silicate solution wear resistance was determined to be higher in the study, the layers corrosion resistances compared, obtained by silica-based electrolyte and more homogeneous and more compact layer with higher corrosion resistance [27].

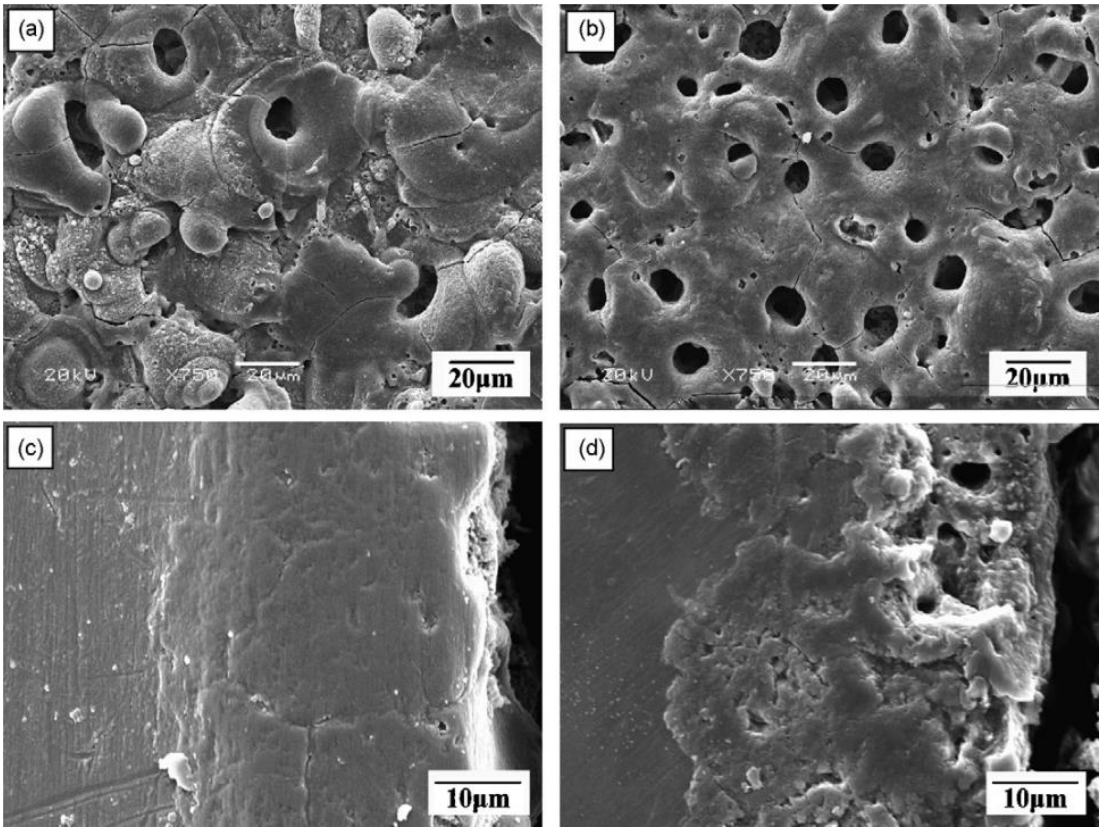

Figure 2.7. SEM images of MAO applied Mg alloys a and b of surfaces and c and d of cross sections [27].

2.3.2. Effect of Rare Earth Metals, MAO and Shot Peening on Corrosion Behavior of Mg Alloys

Magnesium (Mg) alloys have been the attractive light materials to many industrials' applications such as structural components of automotive and aircraft vehicles as a consequence their low g/cm^3 and high MPa/density. AZ31 Mg alloys are the common alloys as commercially, although the weak corrosion which resulted from lower Al content than AZ61 or AZ91 types and poor wear resistance of them hinders their enlarged application areas. in the direction of overcome the unsatisfied corrosion or tribological properties of AZ31 Mg alloys, mainly the coating treatments such as anodizing or micro-arc oxidation (MAO) were utilized to develop both the weak corrosion and poor wear resistances thanks to MgO or Mg2SiO4 [28]. However, the surface treatment of shot peening (SP) mostly was applied to Mg alloys to enhance their fatigue life and wear resistance [29]. By the same token, it is perceived that the SP may be dangerous to corrosion properties of materials in the interest of the high roughness of surface and the used ferrous peening media during SP [30]. The alternative approach to modify the corrosion or wear resistance of Mg alloys is the rare earth metals (REMs) [31]. Moreover, the RE elements play an important role to deactivate impurity and make purer the matrix thus enhancing corrosion resistance effectively [32]. Furthermore, secondary phases reduce the galvanic corrosion where there is a decreasing electrode potential because of the Al11RE3 type secondary phases. Argade G.R. and et. al. studied the Nd added wrought Mg alloys applied oppressive plastic deformation, where it is reported that break-up during deformation of finer and uniformly secondary phases will be effective to the corrosion resistance of Mg alloys [33]. In the literature, Nd mostly was used to reinforce the high-temperature mechanical properties of Mg alloys [34]. However, the stability of secondary phases at higher temperatures can be used as improving wear resistance for Mg alloys. The finer grains can be obtained perfectly via rolling process allowing better corrosion resistance that can be accomplished by using high strain rates or higher rolling speeds [35]. It is reported that the lower strain rates or speeds give rise to twins dominated microstructure, where the corrosion resistance was deteriorated by formed higher stress on the boundaries of twins [18].

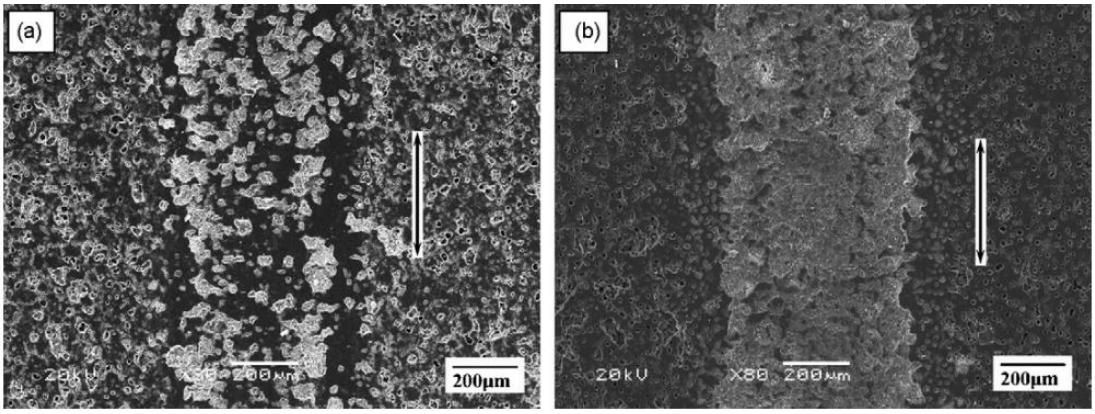

Figure 2.8. SEM images after wear test of MAO applied Mg alloys [27].

PART 3

EXPERIMENTAL STUDIES

3.1. MATERIALS

3.1.1. Casting

In this recent study, AZ31 Mg alloy and modified AZ31 Mg alloys were studied as the main material. The raw materials used for production are given in Table 3.2. Pure Mg, Al pure, pure Zn alloys from Turkey gauges are supplied from China. For the production, a special low-pressure gravity die casting method was used (Figure 3.1) and the casting conditions given in Table 3.1 were complied with. Pure Mg was first introduced into the stainless-steel crucible. After reaching a temperature of 775 ° C, after a waiting period of 1-hour, pure Al and gauge alloys were added to the ladle. Meanwhile, the molten metal in the crucible was continuously stirred. The final alloy addition was added to the pure Zn crucible and after 10 min stirring the molten metal was injected into stainless steel metal molds having a temperature of 355 ° C under 2-4 atm.

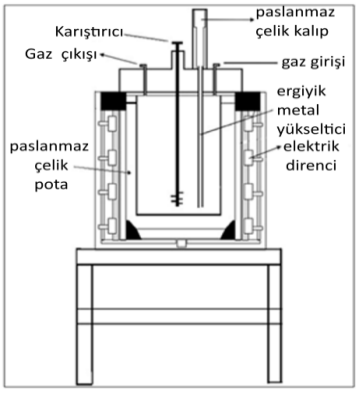

Figure 3.1. Diagram of low-pressure gravity die casting furnace.

Table 3.1. Casting Conditions.

Protective gas	Melting temperature (° C)- Standby time (min)	Mold temperature (° C)	Runner temperature (° C)	Casting gas pressure (Atm)
Argon	775-60	350	350	2-3

Table 3.2. Raw materials used for production (% by weight).

Raw material	Mg	Al	Zn	Mn	La	Nd	Gd
Purified Mg	%99,99	----	-----	----	----	---	---
Purified Al	----	%99,98	-	---	---	---	--
Purified Zn	----	----	%99,989	---	---	---	--
Mastar Mn	%90	---	---	%10	-	-	-
Mastar-La	%70	-	-	-	%30	-	-
Mastar Nd	%70	-	-	-	-	%30	-

The chemical contents of the produced alloys are given in Table 3.3. Rigaku ZSX Primus II device belonging to XRF laboratory of Karabük University Iron and Steel Institute was used for chemical analysis.

Table 3.3. The chemical contents of the produced alloys.

Alloy groups	Materials	Al%wt	Zn%wt	Mn%wt	La%wt	Nd%wt	Gd%wt	Mg%wt
AZ31	AZ31.	2,94	0,987	0,131	-	-	-	Bal.
La	0,2La.	2,963	1,062	0,101	0,212	-	-	Bal.
	0,5La.	3,11	1,06	0,23	0,54	-	-	Bal.
	1La.	2,85	1,02	0,14	0,98	-	-	Bal.
Nd	0,2Nd	2,91	0,97	0,10	-	0,20	-	Bal.
	0,5Nd	2,93	1,03	0,12	-	0,39	-	Bal.
	1Nd	2,93	1,02	0,20	-	0,88	-	Bal.

3.1.2. Rolling

After casting, billets with dimensions of 120x36x12 mm were applied for homogenization heat treatment at 395-410 ° C for 23-24 hours. In order to prevent metal oxidation during homogenization and homogeneous temperature distribution, the materials were embedded in sand. Homogenized materials were hot rolled with parameters in Table 4.4. Here, 15% (total 11 passes) and 30% (total 5 passes) section constriction was applied in each pass. Interpass materials were stored in a furnace at 395-410 ° C for 5-6 minutes. After the narrowing total 83% of the section, billets with initial thickness of 12 mm was reduced to 2 mm thickness.

Table 3.4. Rolling parameters.

<table>
<tr><th>Rolling Temp. (°C)</th><th>Thickness Reduction per pass (%)</th><th>Rolling speed (m/min)</th><th>Total pass number</th><th>Total thickness reduction (%)</th><th>İnitial and final thickness (mm)</th></tr>
<tr><td rowspan="6">400</td><td rowspan="3">15</td><td>1,5</td><td rowspan="3">11</td><td rowspan="6">~83</td><td rowspan="6">12-2</td></tr>
<tr><td>4,7</td></tr>
<tr><td>10</td></tr>
<tr><td rowspan="3">30</td><td>1,5</td><td rowspan="3">5</td></tr>
<tr><td>4,7</td></tr>
<tr><td>10</td></tr>
</table>

3.2. SHOT PEENING

Air-type shot peening treatments with max. 8 bar pressure were carried out according to AISI 1070 after grinded samples with utilizing an air shot- peening machine of TAB firm and metal ball shots Z850 (Ø 850 μm) at steadily lengthy exposure moments (20 minutes) on double side of the sample that impacted 90° of steel ball. the samples of SP’ed were ultrasonically spruced up in methanol to clean dirty particles that coming from the SP process and rests of the ceramic medium.

3.3. MICRO ARC OXIDATION (MAO)

Micro-arc oxidation was applied on samples of rolled AZ31 Mg alloys with dimensions of 25mm*25mm*12mm. The upper area of all the sample was ground using silicon carbide papers # 600 up to # 1200 to certain reliable surface roughness and afterwards cleaned from dirty by ultrasonically with acetone and rinsed with pure water to eschew any surface grimy content prior to the MAO coating practice. A of 2 mm diameter of hole was drilled on the corner of the samples and a thin aluminum rod was utilized to hold the sample and to ensure proper electrical contact. The electrolytic solution was prepared by adding 4g/L of sodium silicate (Na2SiO3), 1g/L of potassium hydroxide (KOH) and 3g/L of disodium hydrogen phosphate (Na2 HPO4) to 4 L of distilled water. The sample of AZ31 Mg(+La, +Nd) alloys arranged for MAO treatment were associated to the (+)terminal of the power source, whereas the (-) terminal was joined to the stainless-steel bath containing electrolyte solution. Amid the MAO proceeding, the electrolyte solution was disturbed steadily by a magnetic mixer to provide legitimate distraction of heat from the electrolyte. Likewise, to preserve the condition consistent, the thorough electrolyte system was wrapped in a custom-made tub through which cold water was spread by an extraneous chiller. An indigenous invented pulsed DC power supply was operated for MAO procedure, which can convey voltage up to 800 V and current up to 20A. With experimental trials, the parameters were decided under constant current and voltage mode at a current density of 85 mA/cm2, frequency of 250 Hz and duty cycle of 10%. A constant voltage regime at a positive voltage 550 and a negative voltage of 100 V. MAO treatment were performed on the specimens for a time duration of 5 minutes.

3.4. CORROSION TEST

Immersion tests were implemented with 3.5% Sodium chloride mix at 25°C. The output of corrosion test were removed using 180 g l-1 CrO3 for 1 minute in ultrasonic cleansing machine and drained by ethonal before mass loss measure. Morphology of the alloys was examined by SEM after immersion test.

3.5. WEAR TEST

The behaviour of dry sliding wear of the SP applied and MAO coated specimens was determined proving a AISI 52100 steel ball of 6 mm diameter. Test procedure was set up according to ASTM G-133. The wear tests were executed at medium conditions at three different loads of 1N, 2N and 5N with an vacillate magnitude of 8 mm and at a sliding velocity of 5 mm s^{-1} for a sliding distance of 50m. Surface roughness and wear depth measurements were performed with a Mitutoyo profilometer. The worn surfaces of samples after wear test were examined by SEM. Further, characterization of the wear trails and the wear wreckage was accomplished in SEM with energy disperse spectra (EDS) analysis tool.

3.6. SURFACE ROUGHNESS TEST

The surface roughness, Ra, of the rolling direction on samples was computed handling surface profilometer (Mitutoya- SVC3200S4 model machine) affirming to ISO 1997 and the surveyed boundary was about 0.08 mm and three reiterations were attended for a moderate value.

PART 4

RESULTS

This section contains the results of test and analysis presented as Table and Figures in following parts.

4.1. PHASE ANALYSIS

The XRD results of investigated alloys was illustrated in Fig. 4.1.

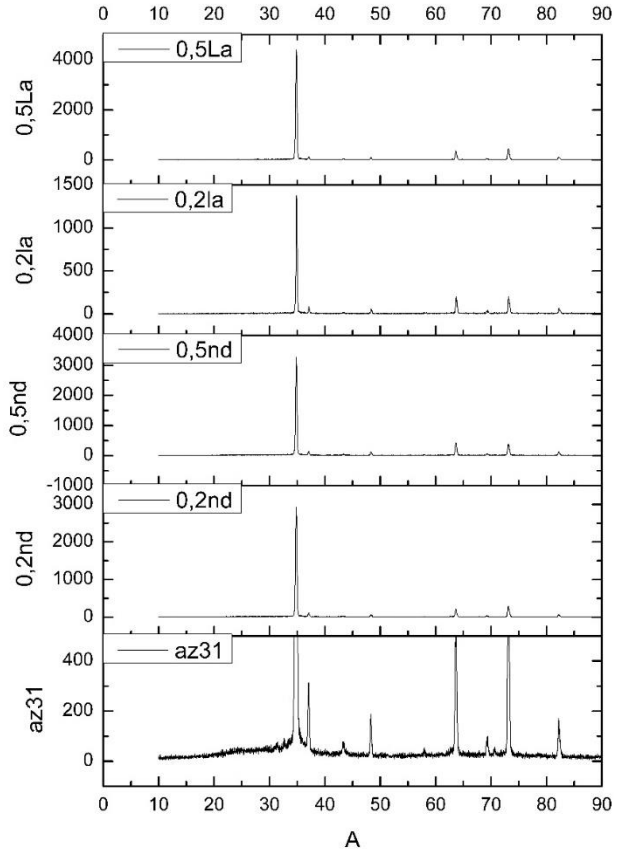

Figure 4.1. XRD templates of MAO coated materials.

4.1. SURFACE ROUGHNESS

Surface roughness of investigated samples was illustrated in Table 4.1.

Table 4.1. The Surface roughness of investigated samples.

Alloys	MAO, 4.7m/min	MAO, 10m/min	SP-MAO, 4.7m/min	SP-MAO, 10m/min
AZ31	2,63	2,898	2,204	2,268
0,2La	2,796	3,226	2,430	3,024
0,5La	3,400	2,458	3,460	2,326
0,2Nd	3,055	3,401	2,308	2,338
0,5Nd	3,022	2,673	2,504	2,181

4.2. CORROSION TEST

The corrosion test results are given in Table 4.2. The corrosion rate and specific corrosion rate were calculated by using of following formula.

Metal loss in unit area.

$$(g/cm^2) = metal\ loss/corroded\ area$$

Specific corrosion rate.

$$(g/cm^2.day) = metallossinunitarea/totalcorrosiontime$$

Table 4.2. Immersion corrosion test results of investigated alloys.

Alloys	Applied process	Metal loss in unit area (mg/ cm^2)							Alloys	Applied process	corrosion rate (mg/ cm^2.hours)						
		24 hr	48 hr.	72 hr.	96 hr.	120 hr.	144 hr.	168 hr.			24 hr.	48 hr.	72 hr.	96 hr.	120 hr.	144 hr.	168 hr.
AZ31	MAO, 4,7	3,584254	5,780387	9,440608	11,6989	15,39365	21,22928	23,76381	AZ31	MAO,4,7	0,149344	0,120425	0,13112	0,121863	0,12828	0,147426	0,141451
	MAO, 10	2,618403	4,485792	7,516915	8,518268	10,66306	16,46143	17,00271		MAO,10	0,1091	0,093454	0,104402	0,088732	0,088859	0,114316	0,101207
	SP-MAO, 4,7	2,556746	5,41316	9,869931	11,02397	14,5116	21,6909	22,88957		SP-MAO,4,7	0,106531	0,112774	0,137082	0,114833	0,12093	0,150631	0,136247
	SP-MAO, 10	2,859195	5,229885	10,07184	11,57328	16,22126	26,42241	27,88793		SP-MAO,10	0,119133	0,108956	0,139887	0,120555	0,135177	0,183489	0,166
0,2La	MAO, 4,7	3,017272	6,802961	14,1699	18,01903	28,36094	33,07719	42,69299	0,2La	MAO,4,7	0,12572	0,141728	0,196804	0,187698	0,236341	0,229703	0,254125
	MAO, 10	2,533333	4	7,161905	8,628571	12,55238	16,59683	17,15556		MAO,10	0,105556	0,083333	0,099471	0,089881	0,104603	0,115256	0,102116
	SP-MAO, 4,7	4,196265	9,015013	25,74881	29,30795	35,98682	40,62981	49,60088		SP-MAO,4,7	0,174844	0,187813	0,357622	0,305291	0,29989	0,282151	0,295243
	SP-MAO, 10	4,687673	8,30293	15,24046	15,64953	25,94804	27,15865	28,96075		SP-MAO,10	0,19532	0,172978	0,211673	0,163016	0,216234	0,188602	0,172385
0,5La	MAO,4,7	2,967742	6,580645	15,40238	23,27334	31,93888	44,14261	47,13752	0,5La	MAO,4,7	0,123656	0,137097	0,213922	0,242431	0,266157	0,306546	0,28058
	MAO, 10	3,25548	5,79231	10,80129	21,09235	27,08588	30,57851	33,91304		MAO,10	0,135645	0,120673	0,150018	0,219712	0,225716	0,212351	0,201863
	SP-MAO, 4,7	2,294294	7,153153	13,62162	19,24324	27,03904	31,88589	39,66967		SP-MAO,4,7	0,095596	0,149024	0,189189	0,20045	0,225325	0,22143	0,236129
	SP-MAO, 10	3,672022	6,349538	9,145281	10,0007	14,90368	25,75979	29,71695		SP-MAO,10	0,153001	0,132282	0,127018	0,104174	0,124197	0,178887	0,176887
0,2Nd	MAO,4,7	2,567523	3,927976	7,102367	11,19707	11,86395	12,6909	13,09103	0,2Nd	MAO,4,7	0,10698	0,081833	0,098644	0,116636	0,098866	0,088131	0,077923
	MAO,10	3,061093	4,154341	4,778135	5,144695	6,745981	10,07717	11,59486		MAO,10	0,127546	0,086549	0,066363	0,053591	0,056217	0,06998	0,069017
	SP-MAO,4,7	2,766025	5,058415	6,820335	12,61762	14,30376	15,16261	16,10988		SP-MAO,4,7	0,115251	0,105384	0,094727	0,131434	0,119198	0,105296	0,095892
	SP-MAO,10	3,528642	4,91653	6,238953	6,98527	9,636661	11,93453	13,6563		SP-MAO,10	0,147027	0,102428	0,086652	0,072763	0,080306	0,082879	0,081288
0,5Nd	MAO,4,7	2,938389	3,893026	5,599188	5,924171	7,664184	9,587001	10,62288	0,5Nd	MAO,4,7	0,122433	0,081105	0,077766	0,06171	0,063868	0,066576	0,063231
	MAO,10	2,797619	4,05506	4,434524	7,202381	9,136905	10,29762	10,46131		MAO,10	0,116567	0,08448	0,061591	0,075025	0,076141	0,071511	0,06227
	SP-MAO,4,7	2,877564	6,109385	8,185208	8,924798	11,734	15,03418	15,58732		SP-MAO,4,7	0,119898	0,127279	0,113683	0,092967	0,097783	0,104404	0,092782
	SP-MAO,10	2,901146	3,796562	5,121777	6,955587	8,065903	8,767908	9,233524		SP-MAO,10	0,120881	0,079095	0,071136	0,072454	0,067216	0,060888	0,054961

.

4.3. WEAR TEST

The wear test results are given in Table 4.3. The wear rate and specific wear rate were calculated by using of following formula.

$$\text{Wear rate; } V(mm^3) = \frac{2}{3} a.b.c$$

Where a and b are the height and width of wear track and c is long of wear track.

$$\text{Specific wear rate; } V(mm^3/m) = wear\ rate\ /\ d.\text{N}$$

Where d is the total distance of wear.

Table 4.3. Wear test results of investigated alloys.

Alloys	Applied process	1N						2N						5N					
		a µm	b, µm	c, cm	d m	Wear rate (2*a*b*c)/3, mm^3	Specific wear rate mm^3/m. N	a µm	b, µm	c, cm	d, m	Wear rate (2*a*b*c)/3, mm^3	Specific wear rate mm^3/m. N	a µm	b, µm	c, cm	d, m	Wear rate (2*a*b*c)/3, mm^3	Specific wear rate mm^3/m. N
AZ31	MAO,4.7	0,45	44	1	50	0,00132	0,00132	1,07	75	0,9	50	0,004815	0,0024075	1,291	84	1,1	50	0,00795256	0,001590512
	MAO,10	0,392	10	1	50	0,000261333	0,000261333	0,888	53	0,98	50	0,003074848	0,001537424	1,283	100	0,99	50	0,0084678	0,00169356
	SP-MAO,4.7	0,4	9	0,9	50	0,000216	0,000216	1,1	70	0,99	50	0,005082	0,002541	1,4	100	1	50	0,009333333	0,001866667
	SP-MAO,10	0,9	45	0,8	50	0,00216	0,00216	1,2	48	1,1	50	0,004224	0,002112	1,31	123	0,95	50	0,0102049	0,00204098
0,2La	MAO,4.7	0,4	10	1	50	0,000266667	0,000266667	0,2	18	1,05	50	0,000252	0,000126	1,5	15	1,1	50	0,00165	0,00033
	MAO,10	0,4	35	0,95	50	0,000886667	0,000886667	0,5	35	1	50	0,001166667	0,000583333	1,1	30	1	50	0,0022	0,00044
	SP-MAO,4.7	0,4	10	0,9	50	0,00024	0,00024	0,98	79	1,2	50	0,0061936	0,0030968	1,1	95	1,2	50	0,00836	0,001672
	SP-MAO,10	0	0	0,8	50	0	0	0	0	0,95	50	0	0	1	60	1	50	0,004	0,0008
0,5La	MAO,4.7	0,81	18	0,99	50	0,00096228	0,00096228	0,68	25	1,05	50	0,00119	0,000595	1,1	90	0,75	50	0,00495	0,00099
	MAO,10	0,8	18	1,3	50	0,001248	0,001248	1	78	1,28	50	0,006656	0,003328	1,27	100	1,3	50	0,011006667	0,002201333
	SP-MAO,4.7	0	0	1,1	50	0	0	0	0	1,15	50	0	0	0	0	1,08	50	0	0
	SP-MAO,10	1,3	15	1,1	50	0,00143	0,00143	0,8	20	1	50	0,001066667	0,000533333	1,3	28	1,15	50	0,002790667	0,000558133
0,2Nd	MAO,4.7	0,7	20	0,9	50	0,00084	0,00084	1,1	68	1	50	0,004986667	0,002493333	1,3	115	1	50	0,009966667	0,001993333
	MAO,10	0	0	0,98	50	0	0	0,6	20	0,99	50	0,000792	0,000396	1,32	100	1,01	50	0,008888	0,0017776
	SP-MAO,4.7	0,8	35	0,99	50	0,001848	0,001848	1,1	78	1,08	50	0,0061776	0,0030888	1,15	118	1	50	0,009046667	0,001809333
	SP-MAO,10	0	0	0,85	50	0	0	0	0	0,99	50	0	0	0	0	1,2	50	0	0
0,5Nd	MAO,4.7	0,72	25	1,25	50	0,0015	0,0015	1,4	105	1,1	50	0,01078	0,00539	1,28	118	1,3	50	0,013090133	0,002618027
	MAO,10	0,02	10	0,8	50	1,06667E-05	1,06667E-05	0,8	70	0,96	50	0,003584	0,001792	1,3	115	0,99	50	0,009867	0,0019734
	SP-MAO,4.7	1,01	50	0,97	50	0,003265667	0,003265667	1	75	1	50	0,005	0,0025	1,3	105	1	50	0,0091	0,00182
	SP-MAO,10	0	0	0,93	50	0	0	0,1	5	0,96	50	0,000032	0,000016	1,3	90	0,99	50	0,007722	0,0015444

The average friction coefficient of investigated alloys is presented in Table 4.4.

Table 4.4. Average friction coefficient of investigated alloys.

Alloys	**Load**	**MAO, 4.7m/min**	**MAO, 10m/min**	**SP-MAO, 4.7m/min**	**SP-MAO, 10m/min**
AZ31	**1N**	0,737	0,687	0,696	0,754
	2N	0,570	0,592	0,669	0,485
	5N	0,578	0,516	0,581	0,345
0,2La	**1N**	0,700	0,461	0,531	0,502
	2N	0,528	0,571	0,269	0,541
	5N	0,516	0730	0,766	0,624
0,5La	**1N**	0,191	0,475	0,492	0,445
	2N	0,278	0,645	0,491	0,458
	5N	0,695	0,729	0,457	0,474
0,2Nd	**1N**	0,720	0,525	0,546	0,476
	2N	0,628	0,581	0,635	0,440
	5N	0,541	0,626	0,714	0,304
0,5Nd	**1N**	0,053	0,674	0,568	0,561
	2N	0,080	0,560	0,663	0,575
	5N	0,113	0,558	0,812	0,647

PART 5

DISCUSSION AND CONCLUSIONS

This section includes immersion corrosion and dry wear test results the graphs which extracted from the test results and analysis. Moreover, some parts contain micrographs to support the discussion.

5.1. IMMERSION CORROSION TEST

To check out the corrosion nature of studied alloys immersion corrosion test for 178 hours was applied. The initial microstructure and the shot peened-coated surface properties was investigated to describe the corrosion attacks which degrade the materials.

5.1.1. AZ31 Mg Alloys

Fig.5.1 displays the coating properties of MAO and SP-MAO applied materials. As seen that the surface roughness of MAO applied sample is more than the SP-MAO one. It can be said that the thickness of material is higher in the condition of the rough surface wherein the coating will show non-homogeneously distribution due to the additional substrates will be added on the island structure during MAO process. Moreover, Tang H. et. al. show that the thickness of coating and the surface roughness of MAO applied samples were increased together. They are found that higher voltage, which is maximum 500 V in their studies is similar with this study, give rise to more erupted molten oxides wherein the filling behavior of spaces of the oxides is brought about and results in enlarged film surface roughness [36].

Coating properties	MAO (µm)	SP-MAO (µm)
R_a	2.62	2.26
Thickness	25	22

Figure 5.1. The coating properties of investigated alloys.

Fig. 5.2 shows that the LOM image of SP-MAO applied AZ31 Mg alloy. It is can be seen finer grains occurred probably due to plastic deformation during shot peening process. Moreover, somewhere of the matrix have DRXs introduced all through the rolling process [37]. Furthermore, Fig. 5.3 illustrates that the SEM images of MAO and SP-MAO samples from their both surface and cross-sections. The surface morphology of SP-MAO sample including more island-structures and volcano-like structures than MAO applied one. Further, SP-MAO sample have bigger and more cracks between the island-structures. The pores were introduced by the molten oxide and gas bubbles discarded of MAO channels and the cracks were formed due to the thermal stresses during rapid solidification [38]. As seen Fig. 5. 3 the cross section of both samples was constituted by outer pores and inner barrier layer. However, compared with the MAO, the SP-MAO sample including more holes like canals that penetrates through of the center of surface.

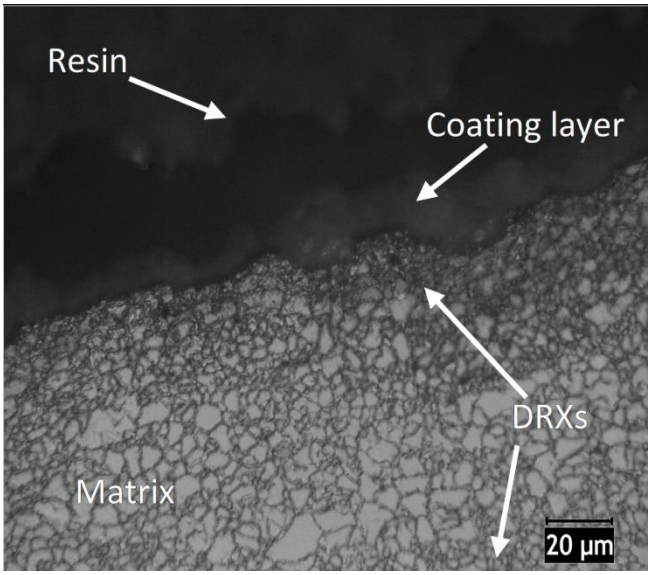

Figure 5.2. LOM image of SP-MAO applied AZ31 Mg alloy.

It is obviously show that the SP changed the MAO coating properties as surface morphology. The surface defects such as macro pores and cracks were unwanted properties which deteriorate of the corrosion behavior of Mg alloys. As seen Fig. 5.3 average pore sizes were calculated by ImageJ software 1,32 µm and 1,476 µm for MAO and SP-MAO samples, respectively. Furthermore, MAO applied sample obtains whiter colored particles especially distributed between island-structures or on them. As seen the Fig.5 the particles including Mg, O and Si or P rich elements.

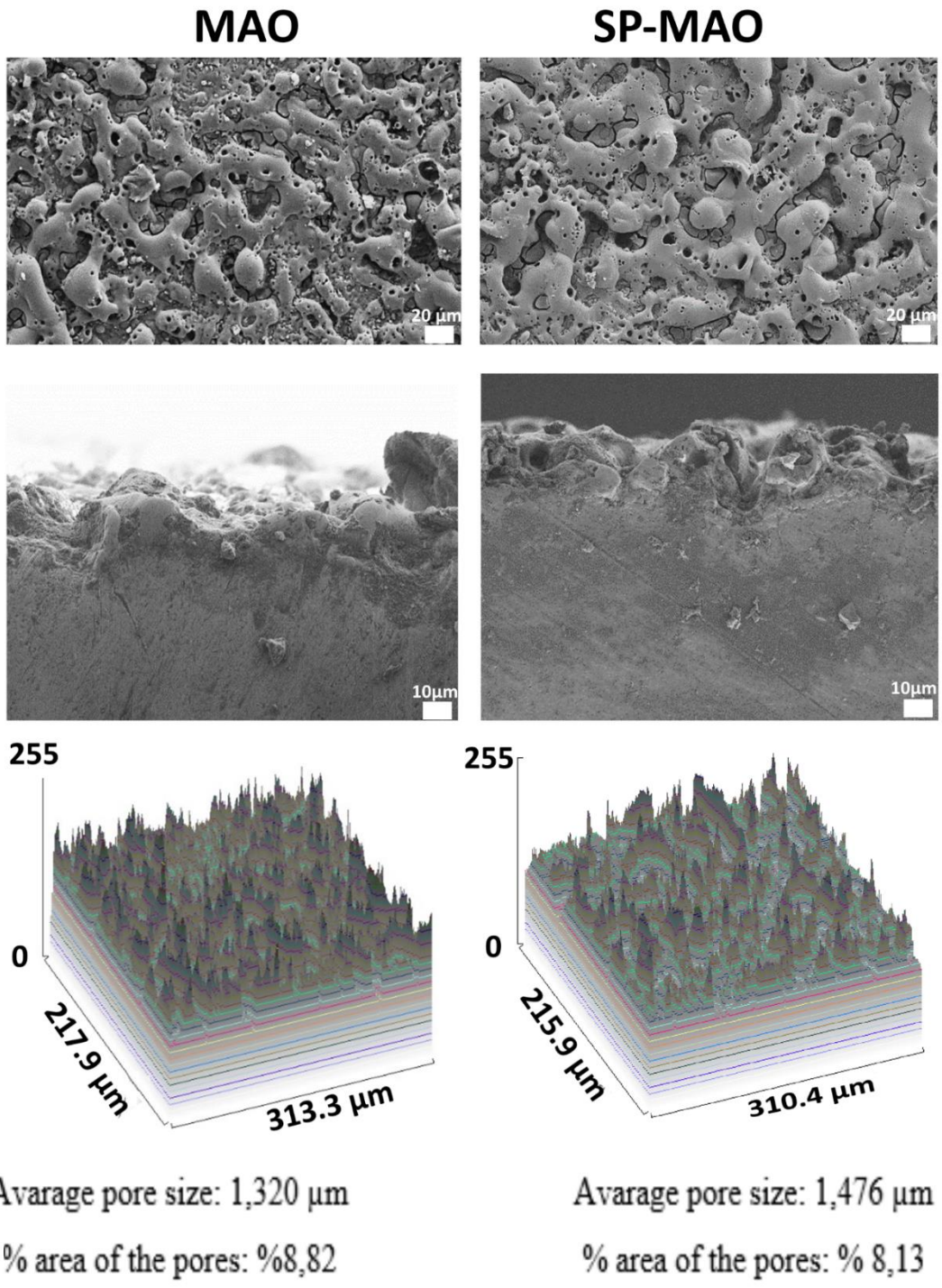

Figure 5.3. SEM images of MAO and SP-MAO samples from their both surface and cross-sections and average pore size and filled area of them on the surfaces.

Fig. 5.4 presents the XRD pattern of MAO applied sample. MAO applied sample demonstrates that the coating was constituted mainly by Mg, MgO and spinel MgAl2O4 phases, in consonance with the alloy composition and the electrolyte. The

existence of the tops of mg was scrutinized, due to the impression from the substrate of AZ31 alloy [39]. Intensity of peaks corresponding to MgO phase increased with increasing concentration of Na3PO4 in the reference electrolyte, while peak intensities of MgAl2O4, α-Mg and β-Mg17Al12 phases decreased conversely. Hence, darkening of the MAO coatings fabricated in Na3PO4 containing electrolytes (Fig. 5. 3) is suggested to be the result of the presence of phosphate containing phase in the MAO coatings.

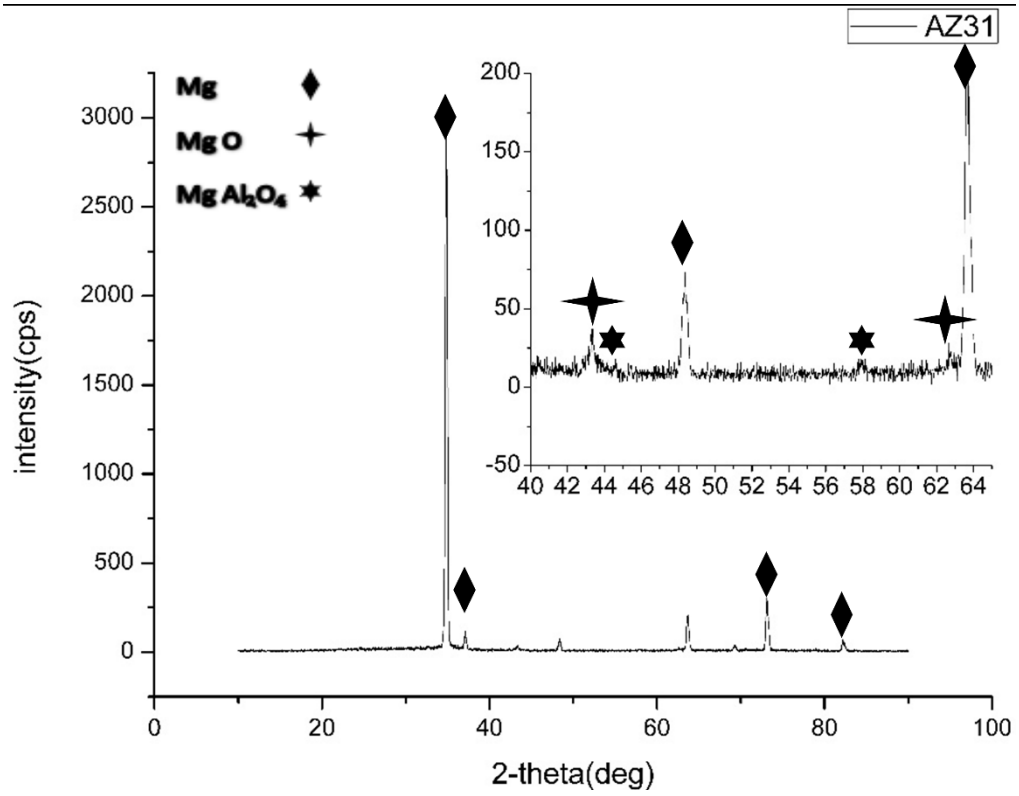

Figure 5.4. XRD pattern of MAO applied sample.

As stated in the obtained data of the XRD analyses (Fig. 5. 4), Al embellished exterior floors of the MAO coatings are gorgeous in spinel MgAl2O4 (which is very hard (about 16 GPa) within the coating), while its Mg gorgeous internal layer is prevailed by MgO. On account of, more extraordinary MgO peaks arose on the XRD spectra (howbeit concentration of MgAl2O4 peaks were weaken) of the MAO coating fabricated in Na3PO4 containing electrolytes (Fig. 5. 3a). It is well ratified that MAO of Mg alloys kickoffs with the MgO evolution by the agency of outward migration of

Mg^{2+} ions from the substrate (AZ31 Mg alloy in this study), which then react with OH^- ions at the metal/electrolyte interface.

As seen Fig. 5. 5, EDS analyses carried out on the surface of MAO applied sample revealed that Mg and O as the main elements as well as Pa Nd Zn and small amounts of Si, Al and K.

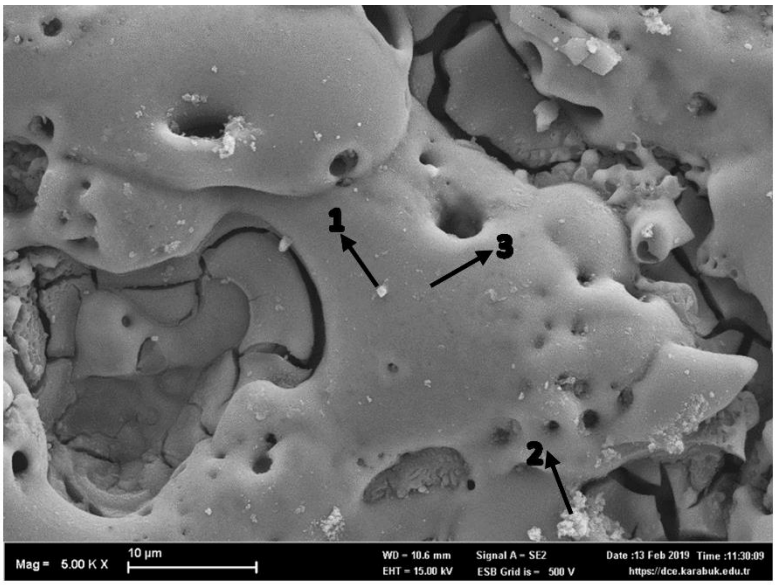

Mass percent (%)

Spectrum	O	Na	Mg	Al	Si	P	K	Zn
1	49.67	1.54	29.18	1.53	5.28	9.57	0.00	3.24
2	51.21	2.42	26.61	0.89	4.76	12.30	0.66	1.15
3	44.03	1.64	33.00	0.97	6.49	12.12	0.22	1.54

Figure 5.5. EDS analysis carried out on the surface of MAO applied sample.

Fig. 5. 6 shows that the corrosion rates of investigated alloys as a Mg loss of unit area versus immersion time of hours in 3.5 wt.% NaCl solution for 168 hours. In the first 24 hours, the metal losses of investigated alloys are approximately similar, however, MAO have less metal loss than SP-MAO. Uncoated AZ31 Mg sheet was immersed for 24 hours showed that 18 mg/cm2 metal loss was reported at our previous study [40]. As seen Fig. 5. 6 the MAO coating is developed the corrosion resistance three times more of AZ31. After 24 hours the metal loss is increasing due to the coating is deteriorated by corrosion attacks wherein the micro-pores and cracks effects the rate

of corrosion as reported by other studies discussed the more sized pores and cracks formation during MAO is important for corrosion speed [41]. Moreover, the port density and size can be evaluated as different subject which determining the corrosion rate of the coating. Higher pore density imparts more electrolytes to penetrate inside of the layer wherein the corrosion attack more degrading. However, if the diameter size of pore is obtained by larger, the corrosion rate will be decreased with the effects of them like corrosion barrier roles. Furthermore, the thickness of the coating gives rise to better corrosion resistance in the case of higher values [3]. Furthermore, the corrosion rate of both samples has increasing slope till 144 hours, however after this time the slope of corrosion rate is decreasing because Mg [OH]2 layer is coating the surface as seen of AZ31 Mg corrosion mechanism. The passive behavior of Mg alloys can be altered by different local pH valued areas wherein the passive film was occurred that making a role as a corrosion barrier. However, chloride environment could be serious attacker for corrosion barriers that resulting pitting corrosion is strongly introduced by surface roughness properties of material. Surface roughness is said that can be detrimental for corrosion resistance because the passivation tendency was interrupted by increased Ra and therefore the alloy more perceptible for pitting corrosion. Nevertheless, the disordered passivity of the alloy imparts lower susceptible pitting corrosion because of the Ra. Our study is appropriate for second one condition of disordered passivity wherein discouraged pitting corrosion impart higher corrosion resistance to MAO applied sample. As reported for Mg alloys, it does not show that urgently formed passive films on the surface wherein the passivity behavior of corrosion is different from aluminum or steel presenting speedily occurred passive films which recovering the corrosion rate immediately. If the surface roughness of Al or steel has high values, pitting corrosion will be finding more site for nucleation. However, the smooth surface give rise to fewer places for pitting corrosion. Further, the passive film ability of the smooth material is better than rougher one that contributing to enhancing of corrosion resistance. On the other hand, Mg does not show quickly formed passive films like Al or steel that changing of surface roughness relationship with the corrosion behavior wherein observed opposite result like the smoother surface are displaying higher corrosion rate due to the passive films does not introduce swiftly [42]. It can be said that the passivity behavior of the MAO coating was changed with the changing of surface roughness wherein it seems like the more

Ra, the less corrosion resistance due to altering of the passivity of MgO or MgAl2O4 on the surface.

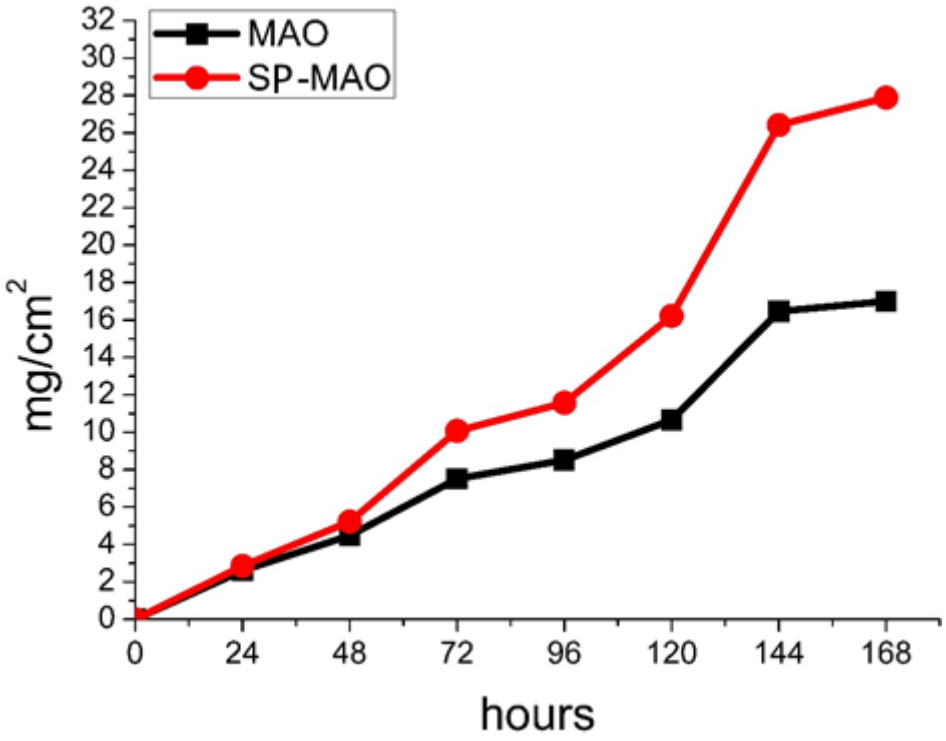

Figure 5.6. Corrosion rates of investigated alloys.

Further, as can be seen from Fig. 5.7 as a result of corrosion attack, surface of the MAO and SP-MAO samples start heavily deteriorated even after 48 hours of immersion. Longer immersion times imposed rough and hollow pit containing surface topography. Surface degradation of the MAO sample was almost small as compared to the SP - MAO sample, if the corrosion pathways appeared on the surface were ignored. Corrosion pathways tended to progress and cover wider surface area at longer immersion durations. On the surfaces of the both samples, indications of corrosion attack were not clearly identified with the exceptions of very fine pits detected mostly at the edges of the samples immersed for 168 hours. Whereas the MAO coating undergoes some severe localized corrosion on its surface (see Fig. 5. 7), indicating that the MAO coating reduces the corrosion of the AZ31 Mg alloy.

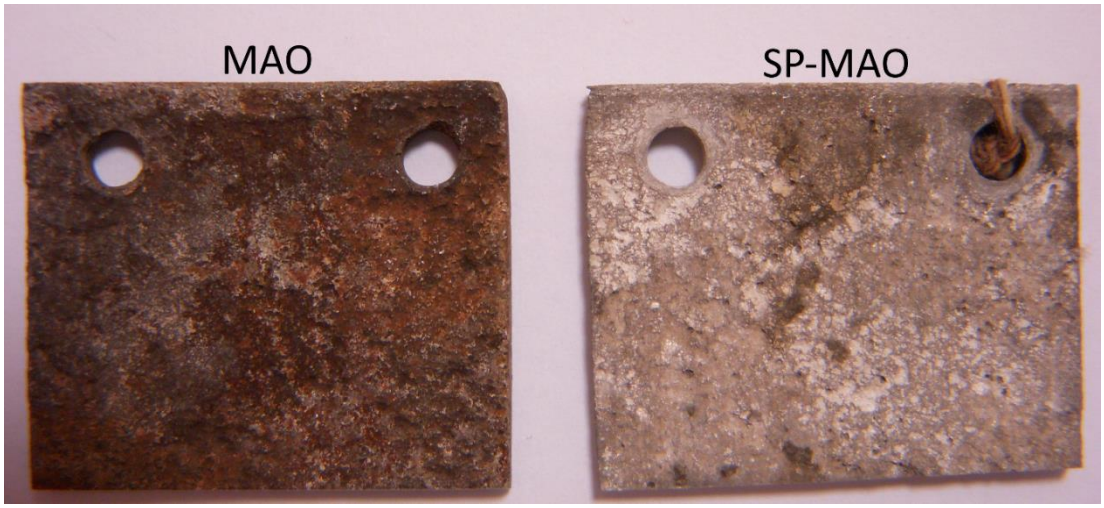

Figure 5.7. The surface morphology after corrosion test.

After corrosion test, SEM examination of corroded surfaces show that the intergranular corrosion mechanism was introduced on the MAO applied sample surface. On the other hand, as seen Fig. 5. 8 the pitting corrosion also was placed on the SP-MAO applied sample.

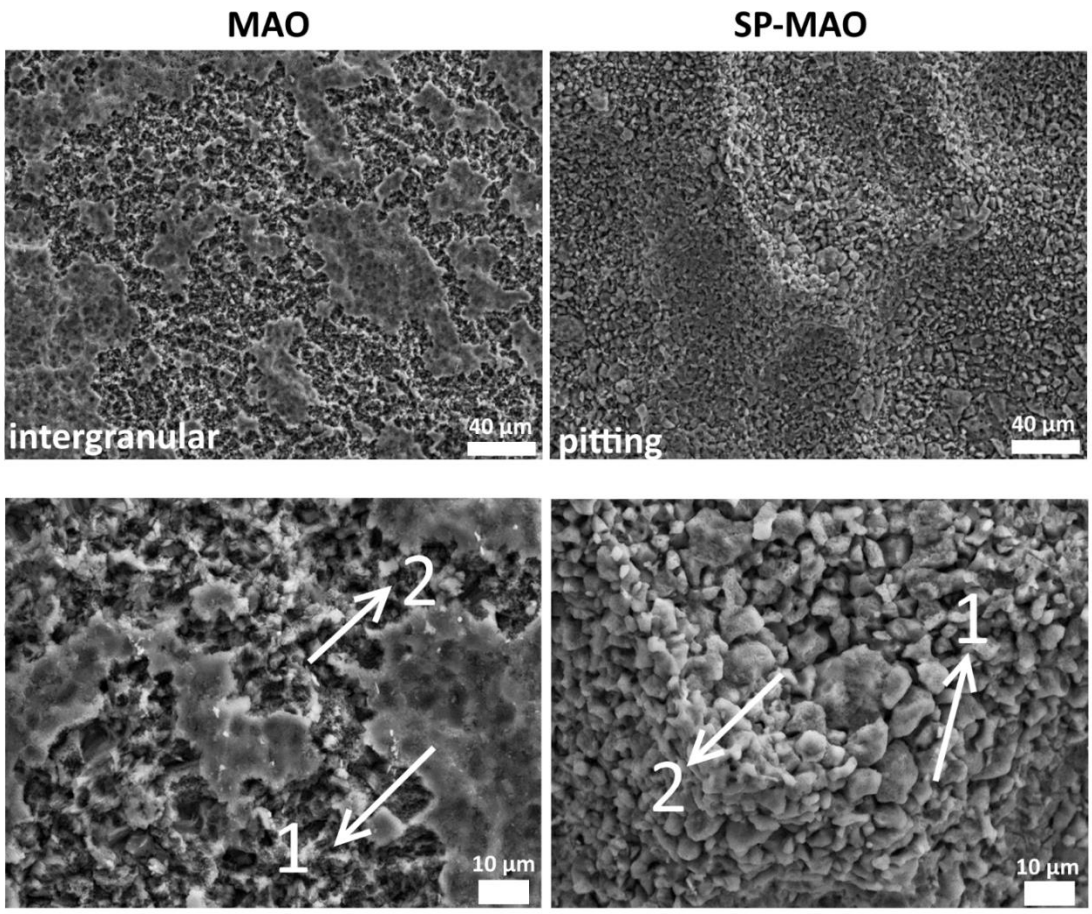

Mass percent (%)

Spectrum	C	O	Na	Mg
1	6.25	14.60	1.18	69.88
2	7.32	7.48	1.42	81.50

Mass percent (%)

Spectrum	C	O	Na	Mg	Si	P
1	11.99	51.15	0.95	24.46	0.75	10.71
2	6.52	1.80	1.42	90.26	-	-

Figure 5.8. The surface SEM images after corrosion test.

After corrosion test, the surface of the corroded surface of both samples includes MgO and C, O and Mg rich areas as seen Fig. 5. 9. Especially the C is more active for find a place in the boundary sections where probably Mg5 [CO3]4[OH] 2.5H2O carbonate product was occurred in the atmospheric condition exposed more carbon on there. It is reported that the mechanism of Mg alloys in the NaCl solution is as following:

$$Mg\ [s] \rightarrow Mg^{2+}[aq]\ + 2e^{-} \tag{5.1}$$

$$2H_2O + 2e^{-} \rightarrow H_2[g] +\ 2OH^{-}[aq] \tag{5.2}$$

$$2H_3O^+[aq] + 2e^- \rightarrow H_2[g] + H_2O \quad (5.3)$$

$$Mg2^+[aq] + 2OH^-[aq] \rightarrow Mg[OH]_2\,[s] \quad (5.4)$$

In the present of CO_{2^-} , $Mg[OH]_2\,[s]$ is converted to magnesium carbonate:

$$5Mg[OH]_2\,[s] + 4HCO_3{}^- + H_2O \rightleftharpoons Mg_5[CO_3]_4[OH_2].5H_2O\,[s] + 4OH^- \quad (5.5)$$

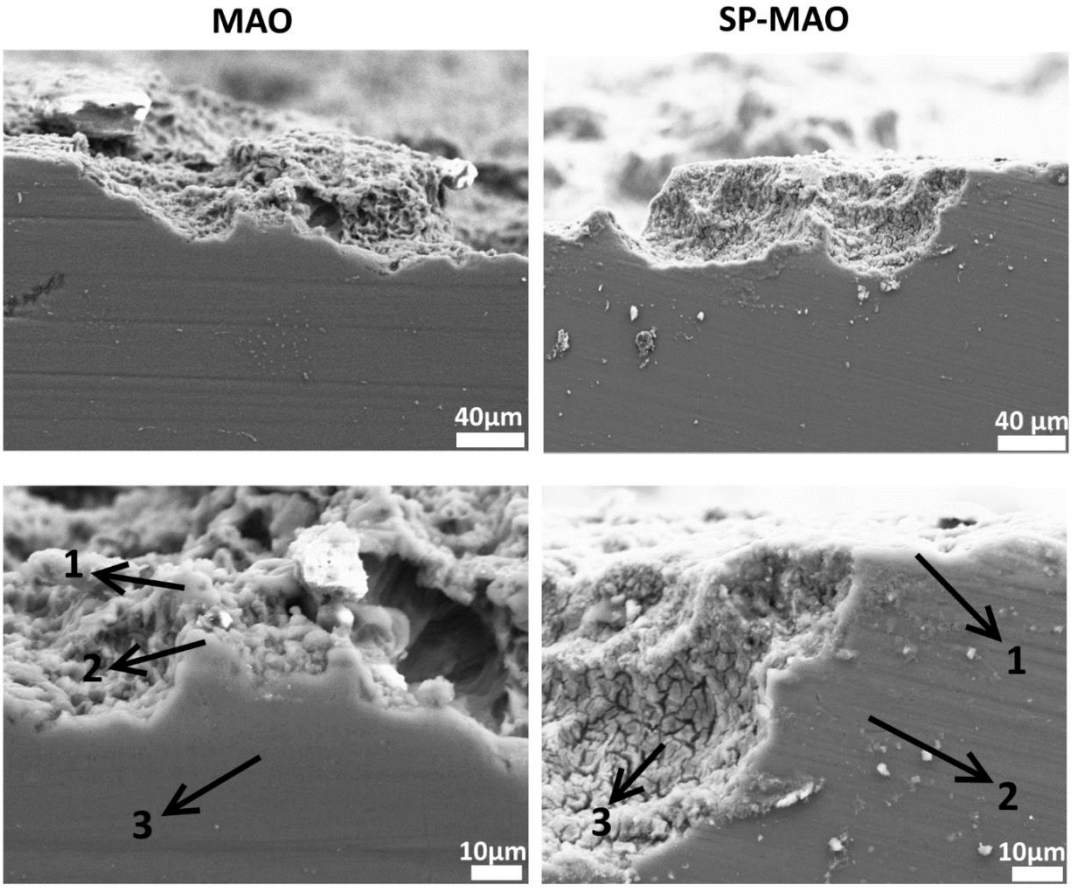

Mass percent (%)

Spectrum	C	O	Na	Mg	Al	Cl	Mn	Zn
1	37.35	30.86	0.94	28.12	1.85	0.15	0.64	0.00
2	75.12	15.24	0.65	8.09	0.64	0.00	0.06	0.19
3	5.09	1.64	0.89	84.12	2.88	0.00	0.43	4.94

Mass percent (%)

Spectrum	C	O	Na	Mg	Al	Cl	Mn	Zn
1	14.25	1.99	1.00	79.23	2.48	0.00	0.04	0.90
2	7.82	1.60	0.76	85.53	2.72	0.00	0.04	1.50
3	7.43	45.83	0.67	31.58	0.96	0.49	3.87	0.72

Figure 5.9. The cross-section SEM images after corrosion test.

The magnesium carbonates are formed as a protective film on the surface that much thicker and more passive than other films such as MgO wherein the corrosion attacks are blocked with them [43]. As seen in Fig. 5. 9, the MAO applied sample consists of higher content of C on the marked as 1 and 2 points. It may be the eliminating factor for corrosion rate therefore the MAO sample lower corroded than SP-MAO one.

5.1.2. AZ31-La Mg Alloys

As shown in Figure 5.10, the base metal of AZ31-0,5La alloys rolled at 4.7 m/min has twins dominated microstructure and bigger sized secondary phases shaped as globular, although the specimen of rolled at 10 m/min speed includes dynamic recrystallization grains also finer secondary phases distributed mostly on grain boundaries as continuously.

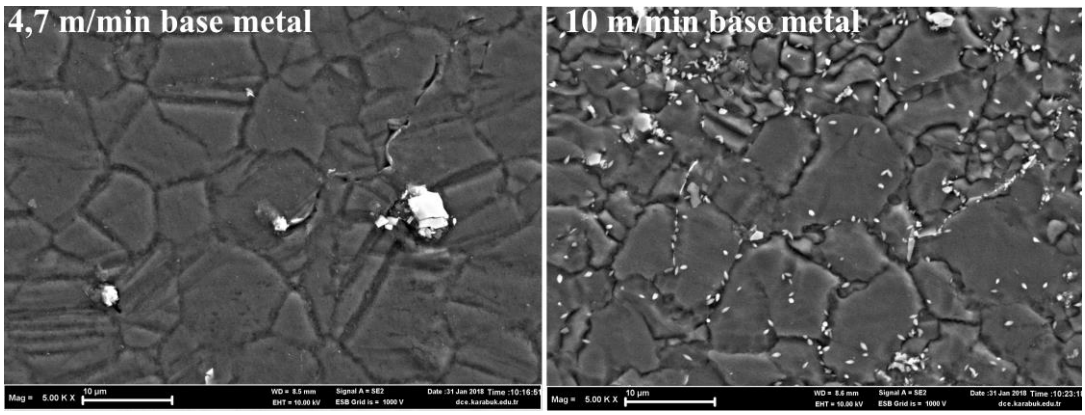

Figure 5.10. SEM images of base metals rolled at 4,7 and 10 m/min.

As shown in Figure 5.11, surface morphology and cross-sectional images of the samples after MAO treatment is different. However, typical coating properties of the MAO process are obtained, for example, from islets of different sizes and micropores of different diameters formed on these islets. Melting and rapid solidification during MAO ensure that the pores are circular. At a rolling speed of 4.7 m / min, the extruded sample has micro-pores with a smaller diameter, however, is denser in the islets. However, it is seen that the rolled material at 10 m / min has larger pores with larger diameters, but they are distributed less on the islets.

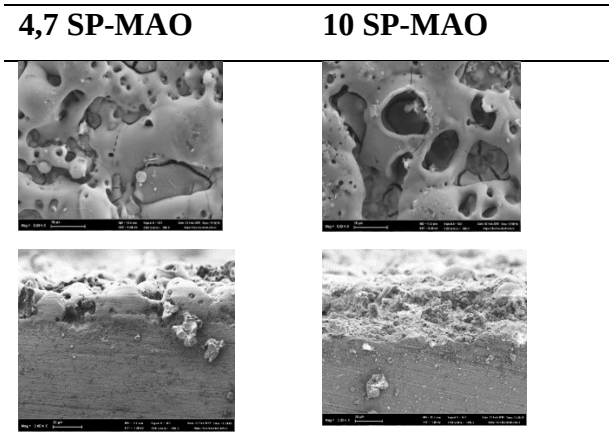

Figure 5.11. SEM images of surface and cross-section of materials at rolled different speeds.

The images taken from the section show us that the rolled material at a velocity of 4.7 m / min is coated non-uniformly, but the coating is more uniform at a speed of 10 m / min. The XRD results of the rolled material at a rolling speed of 4.7 m / min coated with MAO are given in Figure 5.12. It is seen that the coating contains MgO and $MgAl_2O_4$ phases.

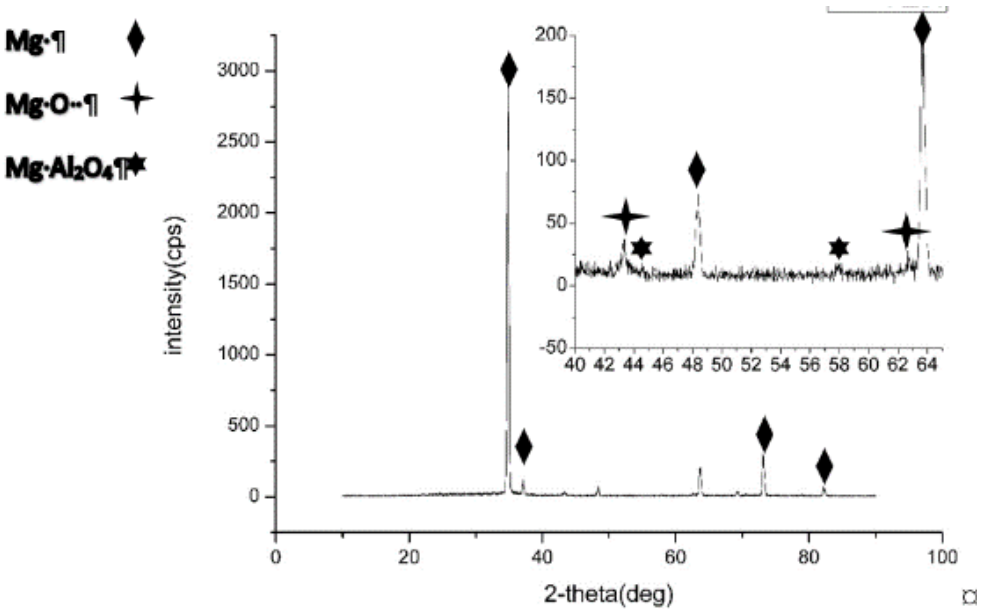

Figure 5.12. XRD patterns of MAO coated material rolled at 4.7 m / min.

5.1.2.1. Surface Smoothness

As can be seen from Figure 5. 13, the surface images of the samples after coating are similar. However, surface smoothness was found to be lower in the rolled material at a rolling speed of 10 m / min.

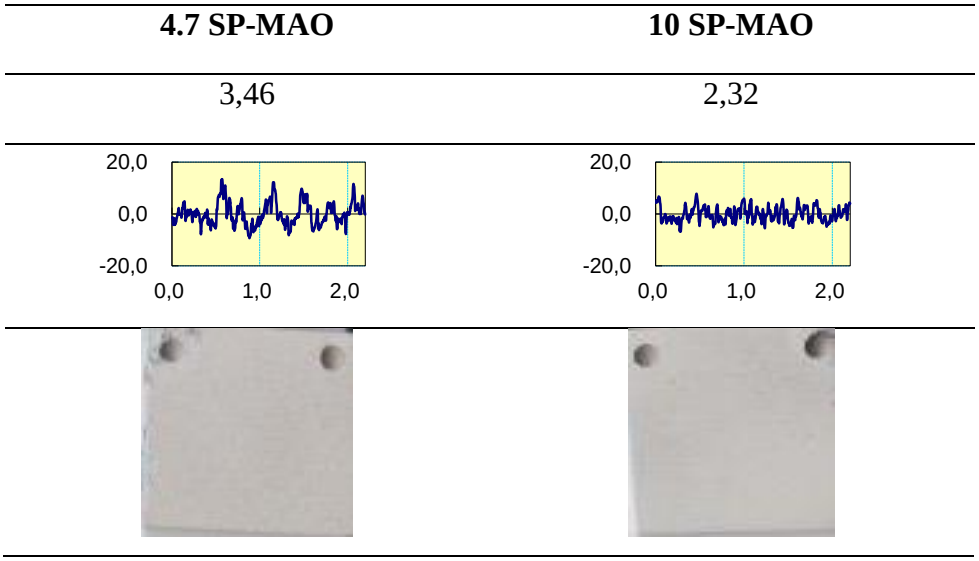

Figure 5.13. Surface properties of the materials examined.

5.1.2.2. Corrosion Test

Immersion test results is shown in Figure 5. 14, the corrosion rate of the rolled material at the rolling speed of 10 m / min to the first 40 hours is faster than that of 4.7 m / min, but after 40 hours, the corrosion rate increased more in the 4.7m / min sample. The corrosion rate of the first 40 hours is under the influence of the coating. However, the corrosion rate was influenced by the properties of the base material in the following hours.

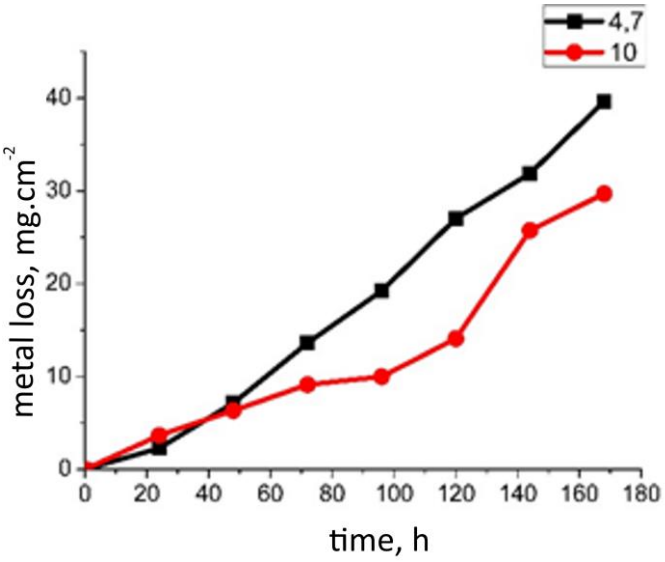

Figure 5.14. Corrosion rates of samples that were corroded for 168 hours in 3.5% NaCl.

The relationship between corrosion rate and MAO coating is determined by the diameter and number of pores the coating has. The more or the larger the diameter, the faster the corrosion tendency. It is believed that the large diameter pores of the rolled material at a speed of 10 m / min cause a high corrosion rate in the first 40 hours. However, it is known that the rolled materials at high speeds contain fewer twins and more recrystallized grains. It is known that twinning adversely affects the corrosion resistance due to the different stress zones they have. However, the fact that the recrystallized grains contain more grain boundaries and less dislocation density contributes to corrosion resistance [35]. The reason why corrosion resistance is weaker after 40 hours in the material with the parameter 4.7 m / min may be attributed to this.

5.1.2.3. After Corrosion

After the corrosion test, pictures and SEM images were taken from the surfaces of the materials and given in Figure 5. 15. As it can be seen from both the macro pictures and the SEM images, it is understood that the rolled material with a rolling speed of 4.7 m / min has deeper and wider corrosion pits.

As can be seen from Figure 5. 16, Mg, O and Al elements remain in the coating material. However, as it progresses towards the base material, Mg becomes more

dominant and O and Al lose the minus. During corrosion, oxidation occurs on the surface of the material and forms a compound with Al and Mg.

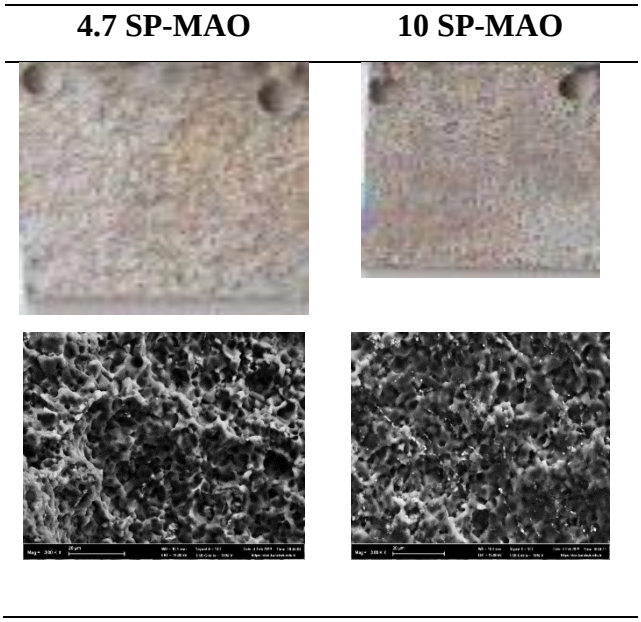

Figure 5.15. SEM investigations after the corrosion test.

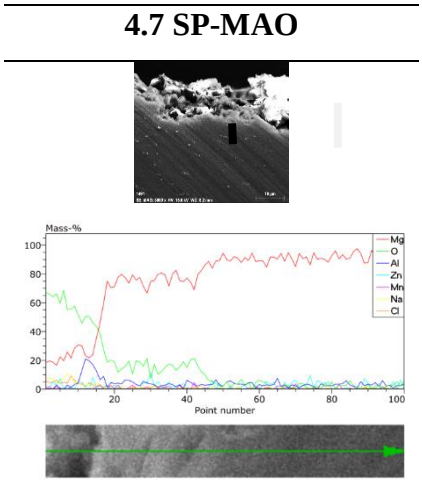

Figure 5.16. Linear EDS analysis from section to base material after corrosion test.

5.1.3. AZ31-Nd Mg Alloys

Fig. 5. 17. demonstrates the immersion corrosion results of investigated alloys during 168 hours in the %3,5 NaCl solution. The initial measure was obtained after 24 hours and the following 24 hours the other values were obtained. It can be seen that the highest metal loss along 24 hours has occurred in a labeled AZ31 sample rolled at 4,7 m/min exposed just MAO treatment on its surface, on the contrary c labeled the same sample include SP-MAO have the lowest metal loss at the same time. At the initial stage of the corrosion test, the resistance of materials could be affected by the morphological differences such as cracks formation or diameter of pores [44]. As seen before the SEM image of a labeled sample, the surface contains a lot of cracks distributed mainly inside the islands and pores have a larger diameter than c labeled samples which includes more homogenously formed ısland (see Fig. 5. 18). The cracks formation can be responsible for the rough surface of just MAO applied AZ31 sample rolled at 4,7 m/min rolling speed. As seen from Fig. 5. 17, the metal loss amount was increasing effectively after 48 hours due to MAO coating is extracted except f,k,l, and n labeled samples. Fig. 5. 19. shows that the specific corrosion rate of investigated samples, there was more corrosion resistance of Nd added alloys than AZ31 Mg alloy. Moreover, the amount of Nd affects the corrosion rate positively. Furthermore, increased rolling speed imparted to more corrosion resistance to samples except the AZ31 alloy rolled at 10m/min with SP-MAO treatments as labeled d in Fig. 5. 19 and Fig. 5. 20 . Illustrates that the secondary phases of AZ31 alloy rolled at different rolling speeds. As seen in Fig. 5. 20 at the 4,7 m/min, the continuously distributed secondary phases more occupied on microstructure and mainly placed on grain boundaries more than 10 m/min. However, twins dominated microstructure deteriorate the resistance of Mg alloys due to the high anodic dissolution which was accelerated by dislocations having a local reduction of equilibrium potential near areas of them. On the other hand, the grain boundaries can be effective to enhance the corrosion, where these grain boundaries act as corrosion barriers [45]. As seen in Fig. 5. 21, DRXs formation mostly occupied the more region of microstructure at 10 m/min than 4,7 m/min rolling speed, in which twins may be the negative factor determine the corrosion resistance after damaged coating.

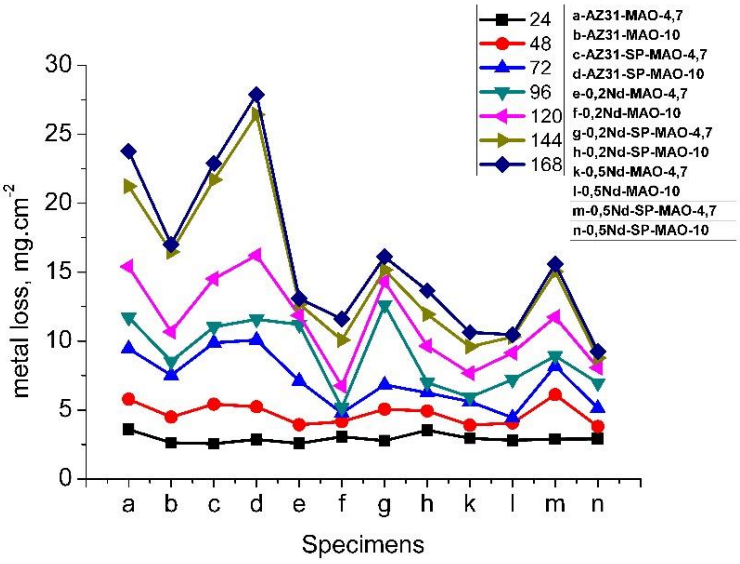

Figure 5.17. The metal loss of specimens for various hours.

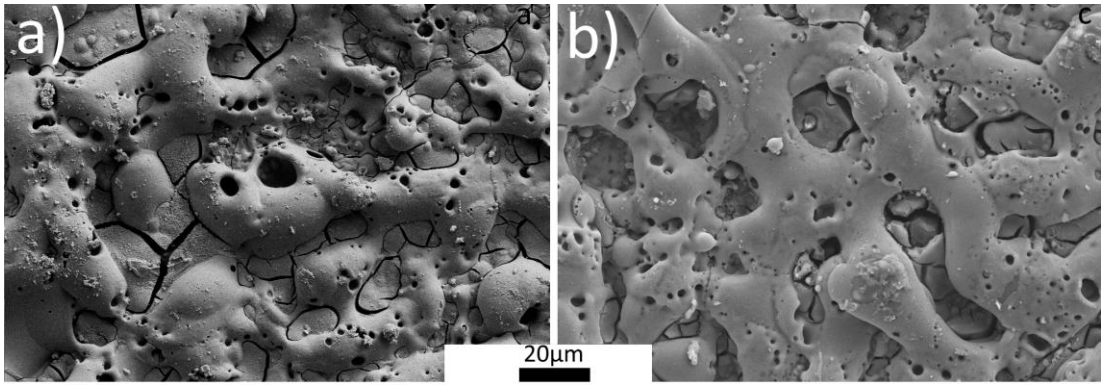

Figure 5.18. SEM surface images of a)MAO coated and b)SP / MAO treated AZ31 Mg alloys rolled at 4,7 m/min speed.

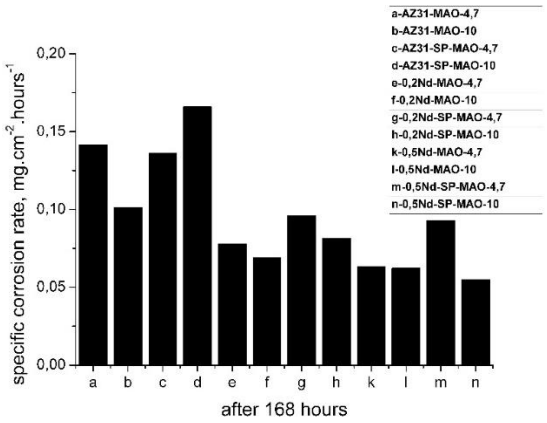

Figure 5.19. Specific corrosion rate of investigated samples.

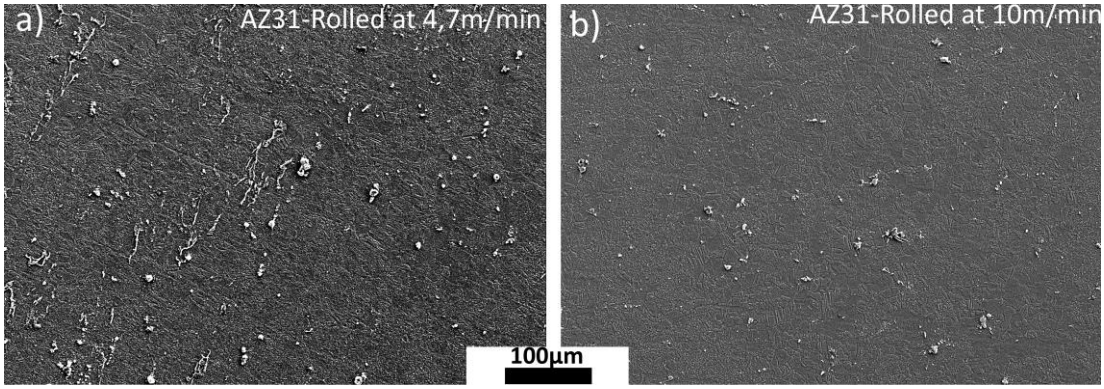

Figure 5.20. Secondary phases of AZ31 alloy rolled at different rolling speed of a)4,7 m/min and b)10m/min.

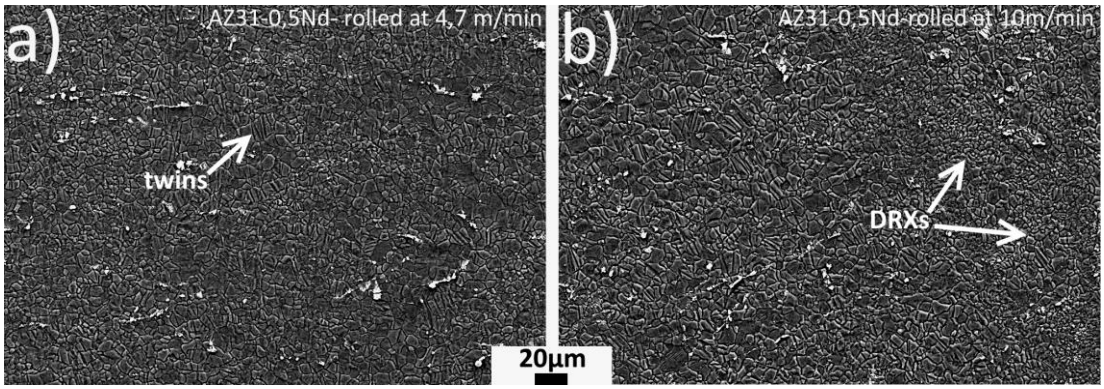

Figure 5.21. Twins and DRXs of AZ31-0,5Nd alloy rolled at different rolling speed of a) 4,7 m/min and b)10m/min.

The SEM images were obtained after the corrosion test of n and d labeled in Fig. 5. 19. that is presented in Fig. 5. 21. n and d labeled alloys before corrosion were rolled at 10 m/min and contains SP and MAO surface treatment. The surface of corroded d labeled alloy of AZ31 was extremely rough as shown in Fig. 5. 22b in which there were vigorously corrosion developed. As illustrated from the enlarged image (Fig. 5. 22b), there are a lot of dimples on the product of corrosion film. During corrosion MgO and Mg (OH)2 layers can be introduced in the film. On the other hand, Mg (OH)2 could be dangerous if it is formed from MgO, wherein the film shows brittle and weak morphology. The environs of Mg(OH)2 were effected by stress extremely due to its volume doubled when it is converted from MgO [46]. As to n labeled alloy of AZ31-0,5Nd, there was a flatter surface than that of d labeled of AZ31 Mg alloy (see Fig. 5. 22a). The film of n labeled alloy includes fewer dimples after the corrosion test, wherein a smooth surface showing less corroded areas. As reported, the surface

roughness after MAO treatment was improved by Nd addition on AZ31 Mg alloy. It is reported that rare earth metals such as Ce can be used as forming a more uniform surface after MAO coating [47]. This study is confirmed that by using of Nd element by our study, the surface of AZ31 after MAO treatment can be obtained highly smooth. The effects of rare earth metals on MAO treatment were reported by the author was developed by decreased active area on the magnesium alloy surface, wherein the rare earth metals react with the other reagents doped in substrate thus cleaning alloy successfully. Moreover, the decreasing active area of the substrate surface could be responsible for strong corrosion resistance because of the rare earth oxides are doped on the Mg alloy surface [48]. Furthermore, compactness of MAO coating could be improved by rare earth elements which are shown enlarged images in Fig. 5. 22a, wherein still flat surface is dominant.

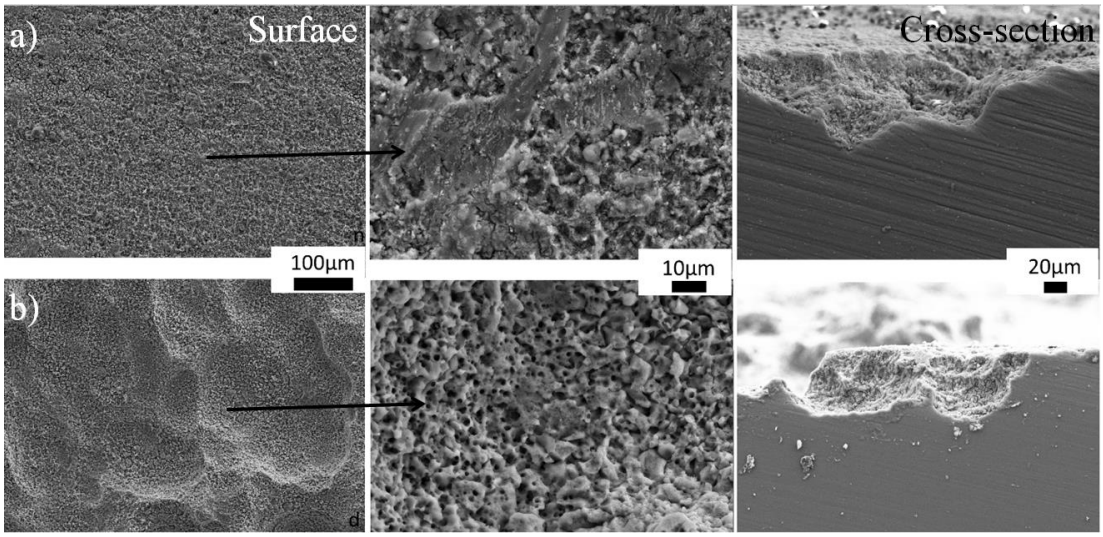

Figure 5.22. SEM images after corrosion test a) AZ31-0,5Nd and b) AZ31 Mg alloys treated with SP and coated by MAO both are rolled at 10m/min.

5.2. WEAR TEST

5.2.1. AZ31 Mg Alloys

The improving of wear resistance of Mg alloys has profound implications for the future of Mg parts as commercially [49]. Shot peening (SP) have been applied to improve fatigue performance of steel, aluminum and titanium alloys [7]. Moreover, the improving of fatigue properties of Mg alloys have been achieved. Higher dislocation density because of work hardening imparts to higher yield strength and hardness during SP, however the surface roughness is deteriorated by SP due to the dents by the shots. Furthermore, the MAO process have been utilized to improve both corrosion and wear resistance of Mg alloys [50]. To decrease the opened porosity and increase the thickness of coating is the popular approach to improve of corrosion and wear resistance of materials [51]. However, the MAO coating on shot peening applied materials have less attention to diminish the wear loss. In this study, the AZ31 Mg alloys was rolled to 2mm thickness with two different rolling speeds following the SP and MAO was applied to improve the wear resistance at room temperature condition. This section contains that the dry sliding wear behavior of the SP applied, and MAO coated AZ31 specimens was determined using an AISI 52100 steel ball of 6 mm diameter. Test procedure was set up according to ASTM G-133 [52]. The wear tests were performed at ambient conditions at three different load levels, viz., 1N, 2N and 5N with an oscillating amplitude of 8 mm and at a sliding velocity of 5 mm s−1 for a sliding distance of 50m. Surface roughness and wear depth measurements were performed with a Mitutoyo profilometer. The worn surfaces of samples after wear test were examined by SEM. Further, characterization of the wear tracks and the wear debris was done in SEM with energy dispersive spectra (EDS) analysis facility [53].

Fig 5.23 and Fig. 5. 24 show the surface morphology and cross-section of the SP-MAO and MAO applied specimens. The aspect of MAO process is formed as pores on both specimens. However, just MAO applied sample also includes cracks which formed especially inside of islands and the size of the pores of MAO is larger than SP-MAO sample. The thickness of coating was obtained as 19,02 μm and 20,74 μm for SP-MAO and MAO samples, respectively. As to the surface roughness value, SP-MAO

applied have value of 2,26 μ, although MAO possess 2,63 μm. These observations can be interpreted as the shot peening impart the surface of AZ31 Mg alloy to deformed layer where valleys are forming during peening. The valleys provide more spaces for MAO particles which was showed yourself us more homogeneous surface morphology and less pores or cracks.

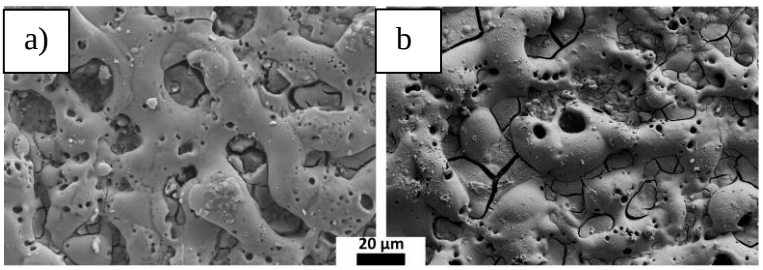

Figure 5.23. SEM of the (a) SP-MAO and (b) MAO applied specimen surfaces.

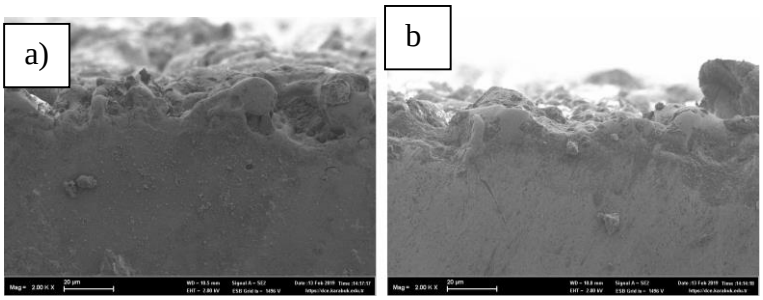

Figure 5.24. SEM of the (a) SP-MAO and (b) MAO applied specimen cross section.

The dry wear behavior of investigated samples illustrated in Fig. 5. 25. affirms that the average friction coefficient values (fcv) for the 1N, 2N and 5N of SP-MAO samples cases were 0.69, 0,66 and 0,58, respectively. As for the MAO applied sample, fcv is higher than for 1N that is 0.73, although fcv is dropping as following value of 0,57 for both 2N and 5N.

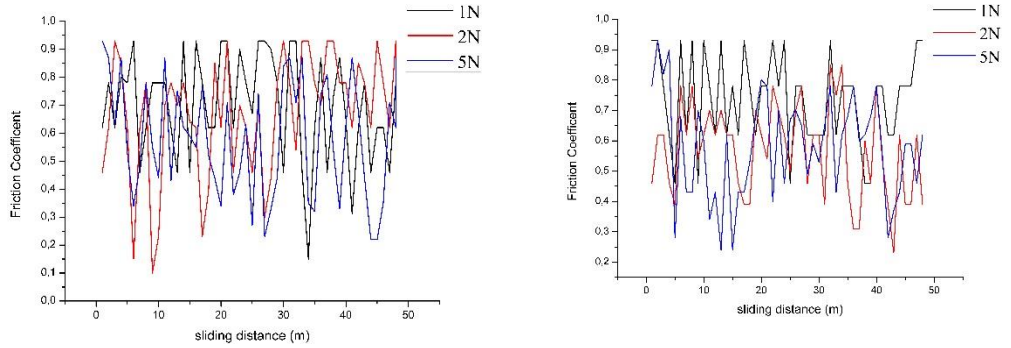

(a) (b)

Figure 5.25. Friction coefficient of the (a) SP-MAO and (b) MAO applied specimens.

The Fig. 5. 26 presents that the wear rate of investigated samples. As seen Fig. 5. 26, particle loss of MAO applied specimen is lower than SP-MAO one in 1N load. Although 2N load removed more particles from SP-MAO applied sample, these values are very close each other. Similarly, the load is 5N the more particles was lifted from SP-MAO applied sample, however the distance between two point is much higher. The denser surface morphology, that means less cracks or pores, give rise minor damage to SP-MAO applied samples as mentioned before lower surface roughness is the main reason for smooth surface. However, it is known that the SP process deteriorate the surface where valley was produced that suffers surface roughness [40]. The main reason could be the change of surface roughness or denser morphology, where if the SR is lower, it will show more wear resistance properties. Higher loads pull off the coating, thus the hard ball contact with inner layers in which the MAO applied sample include more rougher surface than SP-MAO one.

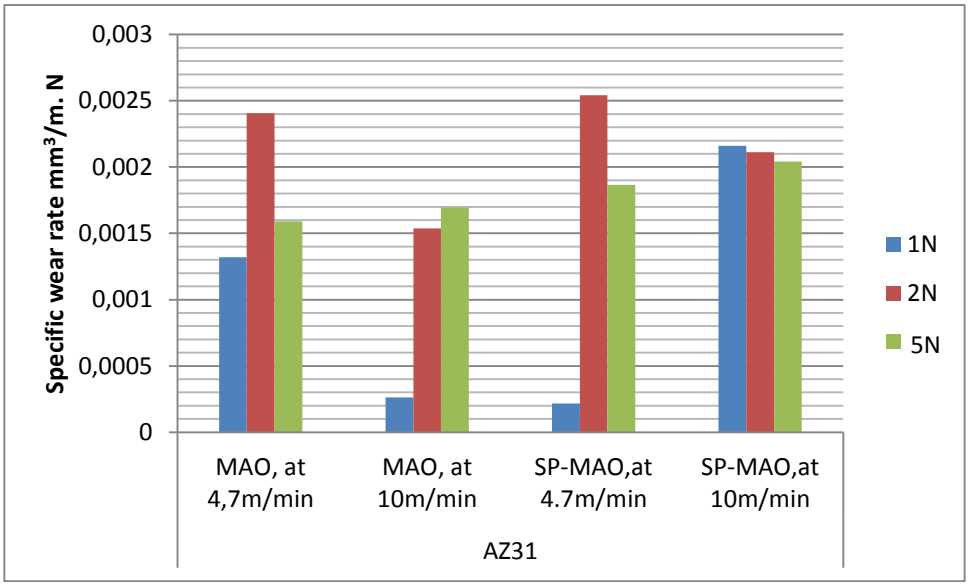

Figure 5.26. Wear rate of the SP-MAO and MAO applied specimens of AZ31.

The wear tracks of the SP-MAO and MAO applied samples which examined by SEM were illustrated in Fig.5. 27. As seen Fig.5. 27, the range of damaged area after wear test is larger for higher loads at both surface conditions. However, the furrows formed in MAO samples develop into deeper and wider, further some particles pull off from the surface of MAO applied in 5N load test. It is known that the hard steel ball easily sank in the soft surface, where fatigue cracks and delamination have been observed. Thus, wear trashes are formed that is noticed primarily in abrasive wear mechanism [54]. On the other hand, there is no wear tracks like grooves in 1N load applied sample of SP-MAO, where especially the surface suffered from scratch on the contrary abrasive or adhesive wear. The main reason for this, the high thicker MAO coating has played an important role of less metal loss, which clearly develops the wear resistance. Moreover, the grooves and ploughs are finer and shallower considering the SP-MAO applied samples than MAO one in 2N load.

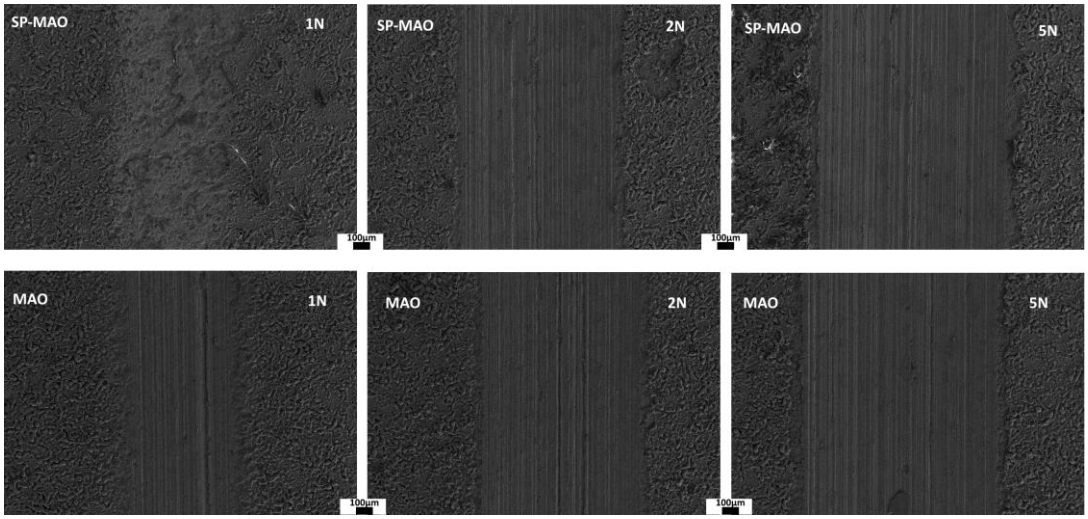

Figure 5.27. SEM of the (a) SP-MAO and (b) MAO applied specimens.

5.2.2. AZ31 – La Mg Alloys

The specific wear rate of La added Mg alloys that were firstly exposed shot peening to increase the hardness and secondly applied the MAO coating to enhance the surface properties such as roughness, hardness and porosity density is presented in Figures 28-30. As seen Fig. 28-30, the wear behavior of added Mg alloys was different based on the applied process to their surface. Moreover, the rolling speed effects the changing of wear rate dramatically. Furthermore, the load amount is the other parameter to understand the wear behavior of the investigated alloys [55].

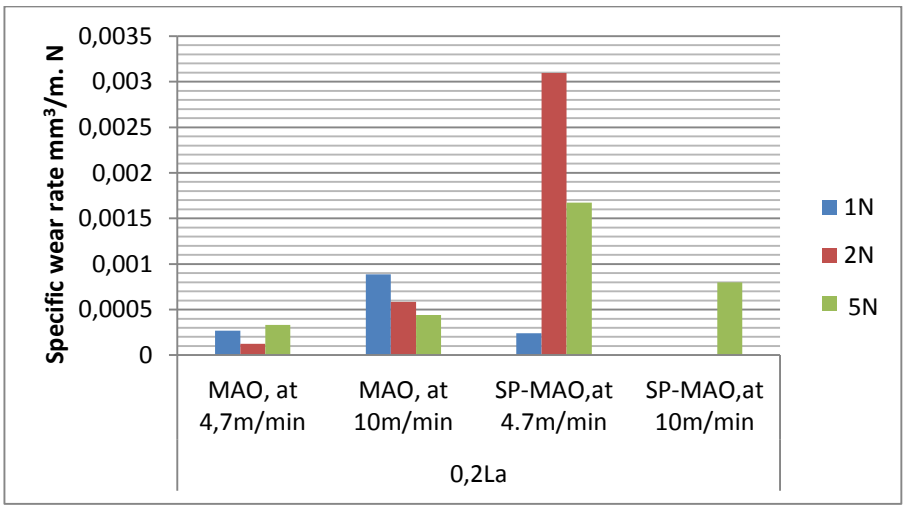

Figure 5.28. Wear rate of the SP-MAO and MAO applied specimens of AZ31 – 0,5La.

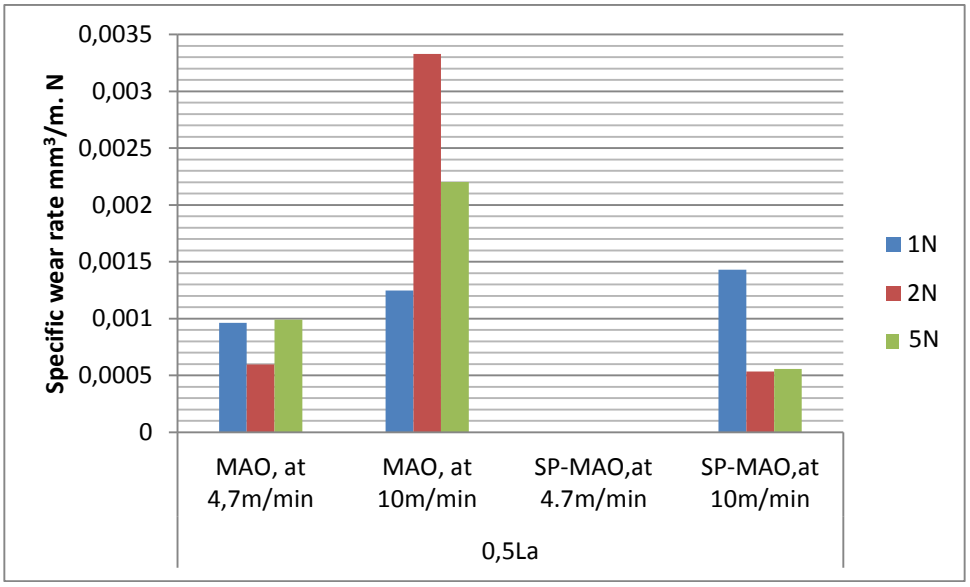

Figure 5.29. Wear rate of the SP-MAO and MAO applied specimens of AZ31 – 0,5La.

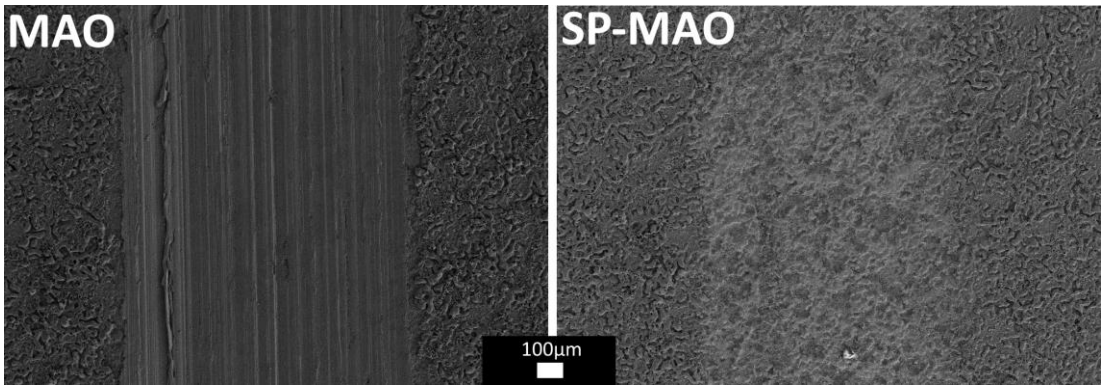

Figure 5.30. After wear test where at applied 2N load, the SEM image of AZ31 – 0,5La Mg Alloys that was rolled at 10 m/min rolling speed.

5.2.2. AZ31 – Nd Mg Alloys

To understand the wear behavior of Nd added AZ31 Mg alloys, 0,2 Nd and 0,5 Nd alloys was closed in graphs. The LOM images of investigated alloys were showed at Fig. 5. 31. As seen Fig.5. 31, both alloys include equiaxed grains however size of some of them is larger of samples deformed at 4,7m/min rolling speed than 10 m/min. Further, the DRXs is a dominant mechanism of rolled samples at 10m/min speed. The CDRXs was just formed at 0,2Nd alloy deformed at 10 m/min speed. However, the shear band was introduced on 0,5Nd added alloy that deformed at 4,7 m/min.

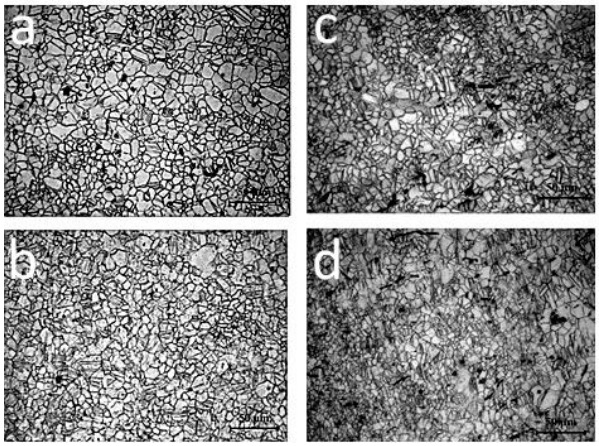

Figure 5.31. LOM images a) 4.7m/min, b) 10 m/min of AZ31-0,2Nd, c) 4.7 m/min and d) 10 m/min of AZ31-0,5Nd.

As presented this Fig. 5.32 the surface roughness is higher for 0,2 Nd added alloys than 0,5 Nd ones (See Fig. 5.32). However, high speed of rolling increased the Ra values of both alloys.

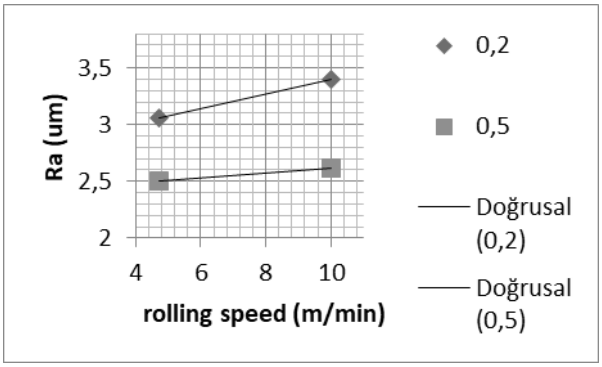

Figure 5.32. Surface roughness of alloys.

SEM images were obtained from surface areas of alloys after MAO process illustrate the holes, cracks and islands (see Fig. 5. 33.). The difference of rolling speed changes the size of holes as seen Fig.5. 33 where diameter size is larger of rolled samples at 4,7m/min, whereas samples of rolled at 10m/min have finer size holes. The islands of samples 10m/min have less holes than 4,7m/min. furthermore, the formation of cracks more observed at 0,2 Nd added alloys.

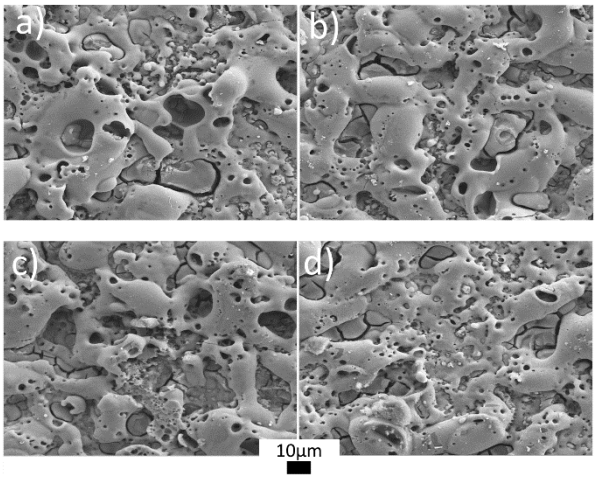

Figure 5.33. SEM images of MAO coated a) 4.7m/min, b) 10 m/min of AZ31-0,2Nd, c) 4.7 m/min and d) 10 m/min of AZ31-0,5Nd.

The wear test results of 0,2 Nd added alloys for deformed at different rolling speeds were showed at Fig. 5. 34. As seen this Fig.5. 34, the metal loss of 4,7m/min alloy occurred excessively more than 10 m/min.

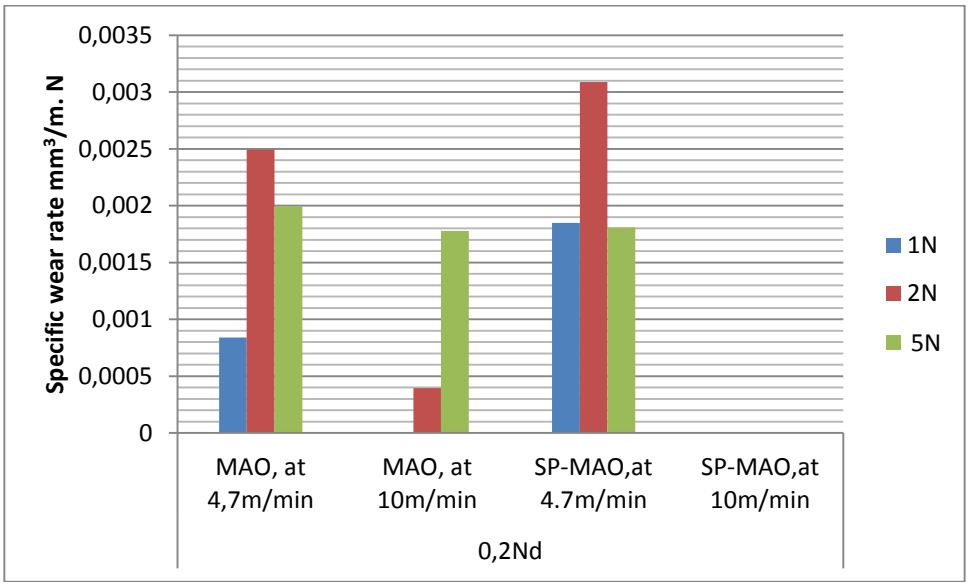

Figure 5.34. Wear test result of 0,2 Nd added alloys.

The wear test results of 0,5 Nd added alloys for deformed at different rolling speeds were showed at Fig. 5. 35 As seen this Fig.5.35, the metal loss of 4,7m/min alloy occurred excessively more than 10 m/min at lower loads. However, the 5N load changed the metal loss amount to increased values for 10 m/min speed rolled sample.

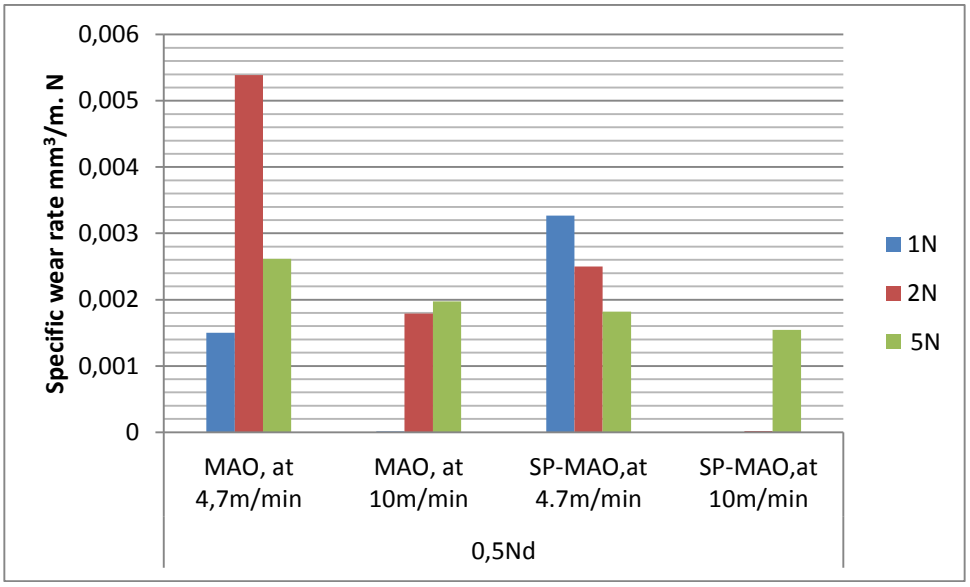

Figure 5.35. Wear test result of 0,5 Nd added alloys.

To compare the wear parameters of all the samples the friction coefficients of the MAO and SP applied MAO coated sliding against the AISI 52100 type bearing steel ball at various loads are showed in Fig. 5. 36. The friction coefficient generally decreased extremely with the loads increasing from 1 to 2N, similarly, friction coefficient has the same reduction when the load increased from 2 to 5N as presented a, b, c, d, e, g, h and l labeled in Fig. 5. 37. This declined maybe since the contact stress decreases with the increase of the contact region. Moreover, the decline of the friction coefficient may be due to the wear mechanism transition caused by the increasing load [53]. Plastic deformation dominates the wear mechanism under high applied loads, which smoothens the surface and decreases the friction coefficient due to the load increases the contact area of the friction pairs increases, and the surface harshness is easily pruned [6].

However, the f, g, k, m, and n labeled samples include increasing friction coefficient with the increase of load. The increase of friction coefficient as a function of load can be due to the wear mechanism transition produced by the increasing load [46].

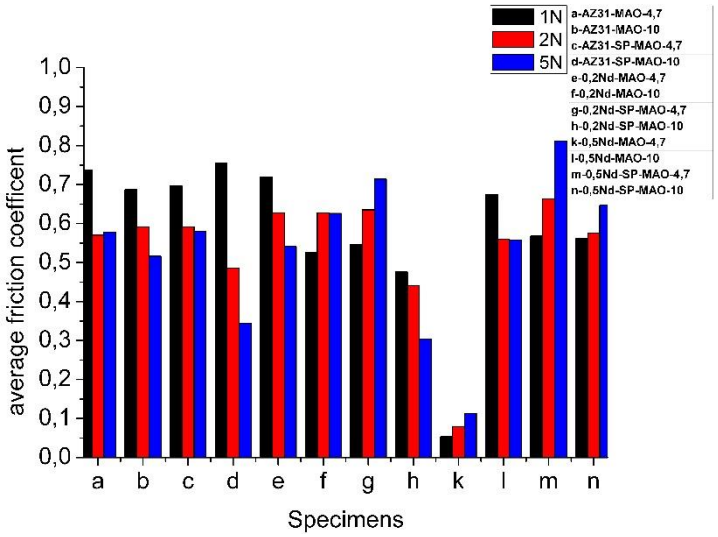

Figure 5.36. Average friction coefficient of investigated alloys.

Fig. 5. 38 is two-dimensional topographies of the wear tracks on the MAO and SP applied/MAO coated samples under different loads. The sliding wear volumes can be obtained by calculating the product of the void areas and the length of the wear scar [54]. It can be clearly seen that both the depth and the width of the wear tracks increased from 1 to 2N loads for k labeled samples, although there is decreasing wear volume from 2 to 5N. It is probably due to the formation of thicker work hardening layers under the applied load of 5 N as compared to 2N. On the one hand, whereas secondary phases still exist on the surface, they cannot be pruned freely by the tangential force from the steel ball due to the work hardening layers stabilize the secondary phases and diminish the evolution of the grooves. On the other hand, the work hardening layers modify the cooperation of the friction pairs and improve the wear performance. The calculated values of sliding wear volumes on MAO and SP applying/ MAO coating caused by sliding wear under different applied loads are shown in Fig. 5.39. It can be seen that as mentioned like k labeled sample, the wear volumes of a,c,e, and g samples under 2N load are larger than samples under 5N load, demonstrating that the secondary phases under 5N are highly compact with work hardening layer, wherein the better wear resistance occurred. On the other hand, other phenomena can be seen from Fig. 5. 39 the increasing loads impart more volume loss to b, f, l, and n labeled alloys. This may be because the rising of the normal load is conducive to the extension of fatigue crack and spalling of the metal surface. Moreover, the hard oxide particles in the MAO coated sample effectively protected

the soft Mg matrix under the low load (1 and 2 N) but failed to function well under the high load (5 N). Furthermore, the oxidation region is porous and brittle, and it is easily sheared from the surface by the higher frictional heat and tangential force. Consequently, the wear rates of the alloys increase with increasing the applied load. As seen in Fig. 5.39 , the decreasingly wear volume loss behavior was obtained from d and m labeled alloys in which volume loss decreased with the increasing from 1 to 5N load, where the work hardening layers as mentioned before fixing the secondary phases which hindering the formation of grooves.

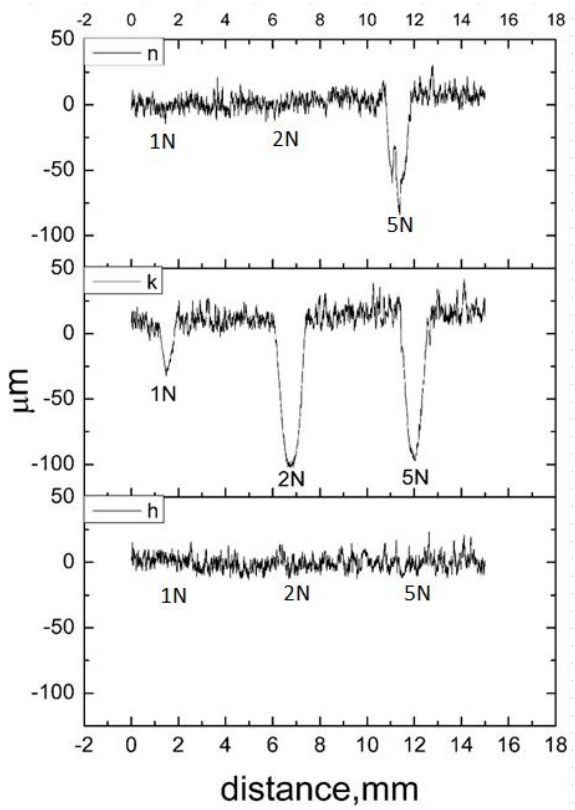

Figure 5.37. Fig. 10. 2D topographies of the wear tracks on the MAO and SP applied/MAO coated samples labeled as n, k and h in Fig. 10.

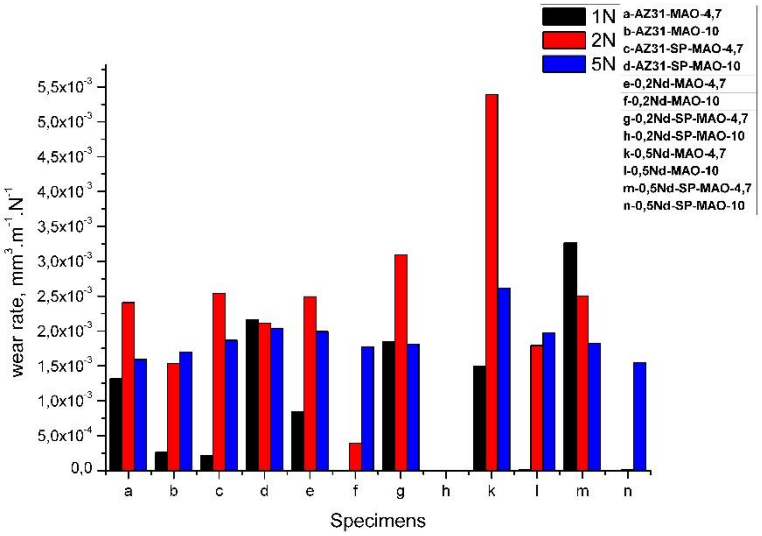

Figure 5.38. Fig. 11. Wear rate of investigated samples.

The worn surfaces under the different loads of 1,2 and 5 N were presented in Fig. 5. 39. It can be detected that various long worn grooves parallel to the sliding direction that are presented on the worn surfaces of 5N load conditions, indicating obvious abrasion and oxidation [56]. Wear debris sticks on shallow grooves were observed at e, g and l labeled samples under 2, 1 and 2N loads, respectively (marked as circled in Fig. 5. 39). Moreover, bright zones introduced as tearing or adhering marks which characteristic is identified as adhesion on samples under mostly force of 5 N. Micro-joints between the disk and the steel ball give rise to the formation of adhesion. Furthermore, oxidation appears at each wear condition except l labeled sample under 1N load, but more oxides form under 5N load (rectangularly marked in Fig. 5. 39).

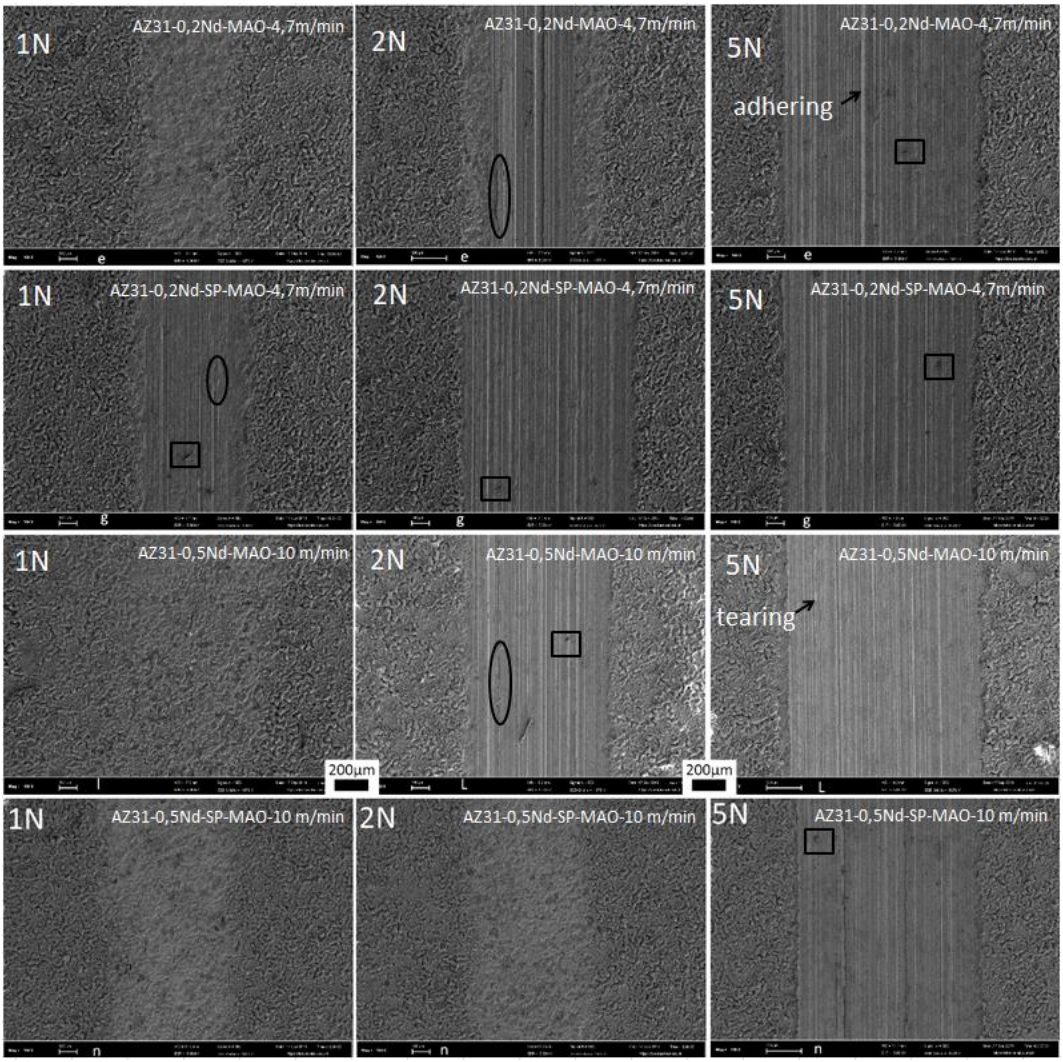

Figure 5.39. The worn surfaces under the different loads of 1,2 and 5 N of MAO coated and SP applied/MAO coated samples of AZ31-0,2 Nd and AZ31-0,5Nd.

Fig. 5. 40 presents the EDX analysis of wear tracks of SP applied and MAO coated AZ31-0,2 Nd alloy and AZ31-0,5Nd alloy under 2N load rolled at 4,7m/min and 10m/min, respectively. The elemental analysis of a rectangular section of a sample of AZ31-0,2 Nd includes O, Mg and Zn rich particles where oxidation wear formed resulting in the content of oxygen elements is very high. Moreover, the wear was damaged by the MAO coating, wherein the Zn element was detected. However, the coating of AZ31-0,5Nd alloy showed more resistance to 2N load, where the O and P amount are highly measured although the Zn is not detected that may be evidence of the wear damaging did not reach the base alloy. In addition, the reason for the high amount of detected O and P is that collected from coating includes potassium hydroxide and there is oxidation formation resulted from the MAO process.

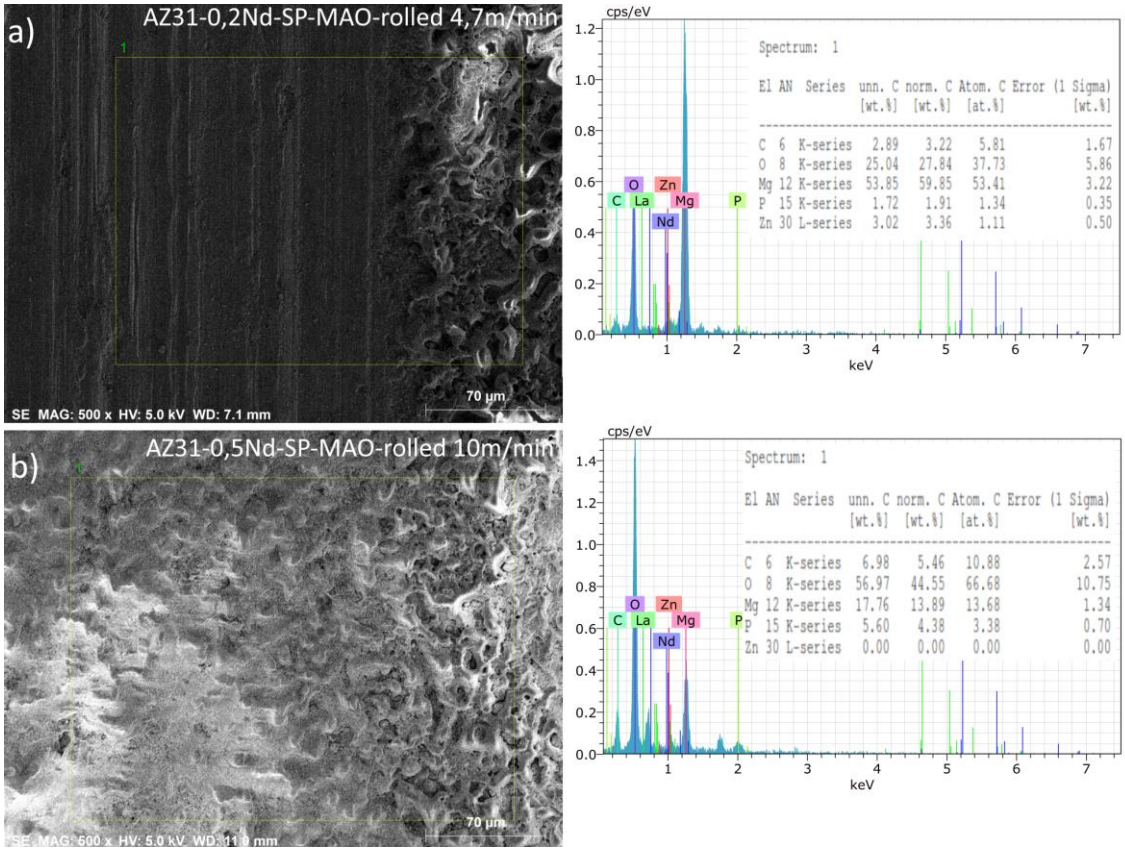

Figure 5.40. Fig. 13. The wear track EDX analysis of SP applied and MAO coated a) AZ31-0,2 Nd alloy rolled at 4,7m/min and b) AZ31-0,5Nd alloy rolled at 10m/min under 2N load.

CONCLUSIONS

- The rolling speeds effect the surface properties of MAO applied Mg alloys as regards surface roughness that have higher values at higher speeds. Similarly, alloying amount of Nd prone change surface roughness to higher values when the amount is higher. Wear rate is proportional to surface roughness for 0,2 Nd alloy which have more metal loss when its Ra values is higher. However, this situation is correct to lower loads for 0,5Nd.

- The surface roughness of MAO coated samples of AZ31 Mg alloys was affected by the pre-treatment of shot peening, the speed of rolling and the amount of Nd. Firstly, the SP imparts to a smoother surface. Secondly, the rolling speed gives rise to the higher rough surface for AZ31 and AZ31-0,2Nd alloys, although the SR showed the decreasing inclination with the increasing rolling speed for the AZ31-0,5Nd alloy. Finally, the lowest SR was measured at 0,5Nd added alloy for all parameters except the SP-MAO applied sample rolled at 4,7m/min.

- The corrosion resistance was improved by the addition of Nd. Initial corrosion attacks find a way to deteriorate the resistance thanks to the crack's formation on the surface after MAO coating. However, the smoothness of the surface developed the corrosion resistance positively. After the damaging of coating, the corrosion resistance of samples was affected by the secondary phases or twins of base materials. The weaker corrosion resistance was observed at twins dominated samples. However, the continuously distributed secondary phases impart to better corrosion resistance due to their barrier effect.

- The general trend of wear coefficients was declining with the increasing load, while that of the mainly Nd added samples presented the rising with the increasing load. As to wear rate, the increasing load from 1N to 2N gives rise

to more metal loss although the 5N load did not wear more metal than 2N due to the compactness of layer mainly effected by work hardening during wear. Oxidations wear mainly observed at the worn surface of samples. However, when the coating was damaged the abrasion is detected dominantly.

- AZ31 Mg alloys were produced by low pressure die casting method following hot rolling process including 4,7 m/min rolling speed and deformation rate per pass is 30%. Furthermore, the wear behavior of SP-MAO and MAO applied AZ31 Mg alloys were investigated at dry condition, the type of wear of the coating were also analyzed. At the conclusion of this study, the wear loss is mainly affected by pores and cracks which deteriorate the surface roughness. In 1N load, the SR impart more wear resistance to SP-MAO applied sample contain less cracks or pores than MAO one. As to 2N and 5N loads, firstly the MAO coating was removed from surface following the change of SR that determined the wear rate of samples. The MAO applied sample has smoother surface than SP-MAO applied, thus the wear resistance of MAO to higher loads is stronger than SP-MAO one.

REFERENCES

[1] Kainer, K., "Magnesium Alloys and Technology", ***Wiley-Vch Verlag GmbH & Co. KGA***, 4-13: Weinheim, (2003).

[2] Mezbahul-Islam,M., Mostafa M., and Medraj, M., "Essential Magnesium Alloys Binary Phase Diagrams and Their Thermochemical Data," 2014: (2014).

[3] Ezhilselvi,V., Nithin, J., Balaraju J., and Subramanian S., "The influence of current density on the morphology and corrosion properties of MAO coatings on AZ31B magnesium alloy," ***Surface and Coatings Technology***, 288: 221-229, (2016).

[4] Yang, J., Peng,J. Nyberg, E., and Pan, F., "Effect of Ca addition on the corrosion behavior of Mg–Al–Mn alloy," ***Applied Surface Science***, 369: 92-100, (2016).

[5] Liu,W., Dong,J., Zhang, P., Korsunsky, A., Song X., and Ding, W. "Improvement of fatigue properties by shot peening for Mg–10Gd–3Y alloys under different conditions," ***Materials Science and Engineering: A***, 528: 5935-5944, (2011).

[6] Asl, K., Masoudi A., and Khomamizadeh, F. "The effect of different rare earth elements content on microstructure, mechanical and wear behavior of Mg–Al–Zn alloy," ***Materials Science and Engineering: A***, 527: 7-8, 2027-2035, (2010).

[7] Champaigne, J. "Shot peening overview," ***Metal Improvement Company***, (2001).

[8] Czerwinski, F. Magnesium Injection Molding, Bolton, Ontario : ***Springer***, (2008).

[9] Tekumalla, S., Seetharaman, S. Almajid, A., and Gupta , M., "Mechanical Properties of Magnesium-Rare Earth Alloy Systems: A Review," ***Metals***, 5: 1-39, (2014).

[10] Martin, É., A "Microtexture Characterization of Recrystallization and Twinning in Magnesium, Montreal": ***Department of Mining and Materials Engineering McGill University*** , (2010).

[11] Taylor, G., and Quinney, H., "The plastic distortion of metals," ***Philosophical Transactions A***, 230: 323-362, (1932).

[12] Styczynski, A., Hartig, C., Bohlen, J., and Letzig, D., "Cold rolling textures in AZ31 wrought magnesium alloy," ***Scripta Materialia***, 50: 7, 943-947.

[13] Chia Ching Hsu E., Effect Of Deformation Conditions On Texture And Microstructure Of Magnesium Sheet Az31, Montreal, Canada : ***McGill***, (2006).

[14] Herrera-Solaz, V., Hidalgo-Manrique, P., Pérez-Prado, M., Letzig, D., Llorca, J., and Segurado, J. "Effect of rare earth additions on the critical resolved shear stresses of magnesium alloys," ***Materials Letters***, 128: 199-203, (2014).

[15] Prasad Narla S., Narasimhan R. and Suwas, S. "Role of Tensile Twinning on Fracture Behavior of Magnesium AZ31 Alloy," ***Magnesium Technology***, 145-150, (2015).

[16] Christian J. and Mahajan,S. "Deformation twinning," ***Progress in Materials Science***, 39: 1-2, 1-157, (1995).

[17] Meng, L. Yang, P., Xie Q., and Mao, W., "Analyses on Compression Twins in Magnesium," ***Materials Transactions***, 49: 710-714, (2008).

[18] Liu, X., Zhu, B., Xie, C., Zhang, J., Tang C., and Chen, Y., "Twinning, dynamic recrystallization, and crack in AZ31 magnesium alloy during high strain rate plane strain compression across a wide temperature," ***Materials Science and Engineering: A***, 733: 98-107, (2018).

[19] Farzadfar, S. A., "Effect of Yttrium on the Microstructure and Texture of Deformed Magnesium", Montreal, Canada : ***McGill University***, (2012).

[20] Guo., L. and Fujita, F. "Effect of deformation mode, dynamic recrystallization and twinning on rolling texture evolution of AZ31 magnesium alloys," ***Transactions of Nonferrous Metals Society of China***, 28: 6, 1094-1102, (2018).

[21] Lee, J., Lee, J., Kim, S., Song, S., Lee C., and Park, S., "Dynamic recrystallization behavior and microstructural evolution of Mg alloy AZ31 through high-speed rolling," ***Journal of Materials Science & Technology***, 34: 1747-1755, (2018).

[22] Nashrah, N., Kamil, M., Yoon ,D., Kim Y., and Ko, Y., "Formation mechanism of oxide layer on AZ31 Mg alloy subjected to micro-arc oxidation considering surface roughness," ***Applied Surface Science***, 497, (2019).

[23] ASTM, Evaluation of Wear Testing, San Francisco: American Society for Testing and Materials, (1968).

[24] Stachowiak G., and Batchelor, A., ***Engineering Tribilogy,*** Waltham, (1993).

[25] Nguyen, Q., Sim,Y., Gupta, M., and Lim, C., "Tribology characteristics of magnesium alloy AZ31B and its composites," ***Tribology International***, 82: 464-471, (2015).

[26] Ilanaganar E., and Anbuselvan, S., "Wear mechanisms of AZ31B magnesium alloy during dry sliding condition," ***Materials Today: Proceedings*** ,5: 628-635, (2018).

[27] Liang, J., Hu, l., and Hao, J., "Characterization of microarc oxidation coatings formed on AM60B magnesium alloy in silicate and phosphate electrolytes," ***Applied Surface Science***, 253: 10, 4490-4496, (2007).

[28] Chen, W.-W., Wang,Z.-x., Lu and Lu, S., "Research of growth mechanism of ceramic coatings fabricated by micro-arc oxidation on magnesium alloys at high current mode," ***Journal of Magnesium and Alloys,*** 3: 253-257, (2015).

[29] Yuan, X., Zhang, J., Lian, Y., Du, C., Xu, W., Zhao, Y., and Mo, J., "Research progress of residual stress determination in magnesium alloys," ***Journal of Magnesium and Alloys***, 6: 238-244, (2018).

[30] Asquith, D., Yerokhin, A., Yates, J., and Matthews, A., "Effect of combined shot-peening and PEO treatment on fatigue life of 2024 Al alloy," ***Thin Solid Films***, 3: 1187-1191, (2006).

[31] Song, Y., Shan, D., and Han, E., "Pitting corrosion of a Rare Earth Mg alloy GW93," ***Journal of Materials Science & Technology***, 33: 954-960, (2017).

[32] Zhu,S., Liu, Z., Qu, R., Wang, L., Li, Q., and Guan, S., "Effect of rare earth and Mn elements on the corrosion behavior of extruded AZ61 system in 3.5 wt% NaCl solution and salt spray test," ***Journal of Magnesium and Alloys***, 1: 249-255, (2013).

[33] Argade, G., Panigrahi S., and Mishra, R., "Effects of grain size on the corrosion resistance of wrought magnesium alloys containing neodymium," ***Corrosion Science***, 58: 145-151, (2012).

[34] Zhang, J., Wang, J., Qui, X., Zhang, D., Tian, Z., Niu, X., Tang, D., and Meng, J., "Effect of Nd on the microstructure, mechanical properties and corrosion behavior of die-cast Mg–4Al-based alloy," ***Journal of Alloys and Compounds***, 464: 1-2, 556-564, (2008).

[35] Fei, G., Dingfei, Z., Xusheng, Y., Luyao, J., Sensen C., and Fusheng, P., "Influence of rolling speed on microstructure and mechanical properties of AZ31 Mg alloy rolled by large strain hot rolling," ***Materials Science and Engineering: A***, 607: 383-389, (2014).

[36] Tang, H., Han, Y., Wu, T., Wei, T., Jian, X., Wu Y., and Xu, F., "Synthesis and properties of hydroxyapatite-containing coating on AZ31 magnesium alloy by micro-arc oxidation," ***Applied Surface Science***, 400: 391-404, (2017).

[37] Galiyev, A., Kaibyshev R., and Saika, T., "Continuous Dynarnic Recrystallization in Magnesium Alloy," 419-422, 509-514, (2003).

[38] Sharma, A., Uma, R., Malek, A., Acharya, K., Muddu M., and Kumar, S., "Black Anodizing of a Magnesium-Lithium Alloy," ***Metal Finishing***, 94:16, (1996).

[39] Guo, H., An, M., Xu, S., and Huo, H., "Formation of oxygen bubbles and its influence on current efficiency in micro-arc oxidation process of AZ91D magnesium alloy," ***Thin Solid Films***, 485: 1-2, 53-58, (2005).

[40] Kara, İ. H., Ahlatcı, H., Türen, Y., and Sun, Y., "Microstructure and corrosion properties of lanthanum-added AZ31 Mg alloys," ***Arabian Journal of Geosciences***, 11: 535, (2018).

[41] Sreekanth, D., Rameshbabu, N., and Venkateswarlu, K., "Effect of various additives on morphology and corrosion behavior of ceramic coatings developed on AZ31 magnesium alloy by plasma electrolytic oxidation," ***Ceramics International***, 6: 4607-4615, (2012).

[42] Alvarez, R. B., Martin, H. J., Horstemeyer, M., Chandler, M., Williams, N., Wang, P. T., and Ruiz, A., "Corrosion relationships as a function of time and surface roughness on a structural AE44 magnesium alloy," ***Corrosion Science***, 5: 1635-1648, (2010).

[43] Lindström, R., Johansson, L., and Svensson, J., "The influence of NaCl and CO2on the atmosphericcorrosion of magnesium alloy AZ91," ***Materials and Corrosion***, 54: 587-594, (2003).

[44] Chen, M. A., Xiao C., and Li, J., "Improvement of Corrosion Performance of MAO Coated AZ31 Magnesium Alloy by Polypropylene Post-treatment," ***Trans. Inst. Met. Finish.***, 91: 80–87, (2013).

[45] Aung, N. N., and Zhou, W., "Effect of grain size and twins on corrosion behaviour of AZ31B magnesium alloy," ***Corrosion Science***, 52: 589-594, (2010).

[46] Gu, Y., Zheng, X., Liu Q., and Yang, D., "Investigating Corrosion Performance and Corrosive Wear Behavior of Sol–gel/MAO-Coated Mg Alloy," ***Tribology Letters***, (2018).

[47] Lı, J., Tian, Y., Gui Z., and Huang, Z., "Effects of rare earths on the microarc oxidation of a magnesium alloy," ***Rare Metals***, 27: 50-54, (2008).

[48] Liu, F., Lı, Y., Gu,J., Yan,Q., Lou, Q., and Cai, Q., "Preparation and performance of coating on rare-earth compounds-immersed magnesium alloy by micro-arc oxidation," ***Transactions of Nonferrous Metals Society of China***, 22: 1647-1654, (2012).

[49] Çuğ, H. and Ahlatçı,H., "Effect of Zn and Mn Additions on the Wear Resistance of Cast Alloy Mg–5% Al–1% Si," ***Metal Science and Heat Treatment***, 59: 3-4, 161-167, (2017).

[50] Khan, S. A., Bhuiyan, M. S., Miyashita, Y., Mutoh, Y., and Koike,T., "Corrosion fatigue behavior of die-cast and shot-blasted AM60 magnesium alloy," 528: 4-5, 1961-1966, (2011).

[51] Gray, J., and Luan, B., "Protective coatings on magnesium and its alloys — a critical review," ***Journal of Alloys and Compounds***, 336: 88–113, (2002).

[52] Nouri, M., Sun, X., and Li, D., "Beneficial effects of yttrium on the performance of Mg–3%Al alloy during wear, corrosion and corrosive wear," 67: 154-163, (2013).

[53] Sun, X., Nouri, M., Wang, Y., and Li, D., "Corrosive wear resistance of Mg–Al–Zn alloys with alloyed yttrium," 302: 1-2, 1624-1632, (2013).

[54] Aydın, F., and Sun,Y., "Investigation of wear behaviour and microstructure of hot pressed TiB2 particulate reinforced magnesium matrix composites," ***Canadian Metallurgical Quarterly***, 57: 455-469, (2018).

[55] Asl, K., Masoudi, A., and Khomamizadeh, F., "The effect of different rare earth elements content on microstructure, mechanical and wear behavior of Mg–Al–Zn alloy," ***Materials Science and Engineering : A***, 527: 7-8, 2027-2035, (2010).

[56] Chen, H., and Alpas, A., "Sliding wear map for the magnesium alloy Mg-9Al-0.9 Zn (AZ91)," ***Wear***, 246: 106-116, (2000).

[57] Walter, R., and Bobby Kannan, M., "Influence of surface roughness on the corrosion behaviour of magnesium alloy," ***Materials and Design***, 32: 2350-2354, (2011).

[58] Imandoust, A., Barrett, C., Al-Samman, T., Inal, K., and El Kadiri, H., "A review on the effect of rare-earth elements on texture evolution during processing of magnesium alloys," ***Journal of Material Science***, 52: 1-29, (2017).

[59] Gusieva, K., Davies, C., Scully, J., and Birbilis, N., "Corrosion of magnesium alloys: the role of alloying," ***International Materials Reviews***, 60: 169-194, (2015).

[60] Rong-chang, Z., Jin, Z., Wei-jiu, H., Dietzel, W., Kainer, K., Blawert, C., and Wei, K., "Review of studies on corrosion of magnesium alloys," ***Transactions of Nonferrous Metals Society of China***, 16: 763-771, (2006).

[61] Tjong, S., and Lau, K., "Properties and abrasive wear of TiB2/Al-4% Cu composites produced by hot isostatic pressing," 59: 2005-2013, (1999).

[62] Hong, E., Kaplin, B., You, T., Suh, M.-S., Kim, Y.-S., and Choe, H., "Tribological properties of copper alloy-based composites reinforced with tungsten carbide particles," ***Wear***, 270: 591-597, (2011).

RESUME

Galal Elmensouri was born in Libya in 1971 and he graduated first and elementary education in the city of Zwara. He completed high school education in Zwara High School, after that, he started undergraduate program in Tripoli University Department of Material science in 1989. Then in 2008, he got the master's degree in material and metallurgical engineering from Sudan Academy for Sciences and then he started assignment as a faculty member in High institute of engineering in Zwara Department of Material science engineering. To complete his Ph.D. education, he moved in 2016 to the Karabük University, where he has been working to get the degree.

CONTACT INFORMATION

Address : Karabük University
Graduate School of Natural & Applied Science
Demir-Çelik Campus/KARABUK
E-mail : galal_mansouri@yahoo.com